Nucleation and arrest of dynamic slip on a pressurized fault

Dmitry I. Garagash[1] and Leonid N. Germanovich[2]

Received 7 February 2012; revised 16 August 2012; accepted 19 August 2012; published 26 October 2012.

[1] Elevated pore pressure can lead to reactivation of slip on pre-existing fractures and faults when the static Coulomb failure is reached locally. As the pressurized region spreads diffusively, slip can accumulate quasi-statically (paced by the pore fluid diffusion) or dynamically. In this work, we consider a prestressed fault with a locally peaked, diffusively spreading pore pressure field to study (1) conditions leading to the escalation of slip and nucleation of dynamic rupture and (2) rupture run-out distance before it is arrested. Nucleation appears in this model when the fault friction decreases from its peak value with slip, while arrest of dynamic propagation is imminent on aseismic faults (i.e., such that prestress τ^b is less than the residual fault strength τ_r at ambient conditions). When fluid overpressure is a small-to-moderate fraction of the ambient value of normal effective stress (and prestress is large enough for fault slip to be activated by overpressure), dynamic rupture always nucleates, and the nucleation length increases with decreasing prestress practically independently of the overpressure value. Transition from the ultimately unstable ($\tau^b > \tau_r$) to the ultimately stable ($\tau^b < \tau_r$) fault loading is marked by a strong increase of the nucleation length ($\propto 1/(\tau^b - \tau_r)^2$) as τ^b approaches τ_r from above. For aseismic faults ($\tau^b < \tau_r$), no dynamic rupture is nucleated at large fluid overpressures for all but the smallest values of prestress. The largest run-out distances of dynamic slip on aseismic faults correspond to overpressure/prestress just sufficient for slip activation. In such cases, the dynamically accumulated slip can lead to enhanced, dynamic fault weakening, resulting in a sustained dynamic rupture and generating a large earthquake. This is consistent with field observations when the largest injection-induced seismicity occurred after fluid injection ended.

Citation: Garagash, D. I., and L. N. Germanovich (2012), Nucleation and arrest of dynamic slip on a pressurized fault, *J. Geophys. Res.*, *117*, B10310, doi:10.1029/2012JB009209.

1. Introduction

[2] Locally elevated pore pressure is a viable mechanism for reduction of fault strength and earthquake triggering. Possible sources of elevated pressure near faults, which are associated with induced or triggered seismicity, include (1) deep fluid injection into the crust for geological storage [*Healy et al.*, 1968; *Raleigh et al.*, 1976; *Zoback and Harjes*, 1997] and stimulation of geothermal and hydrocarbon reservoirs [*Pearson*, 1981; *Warpinski and Teufel*, 1987; *Cornet et al.*, 1997; *Rutledge et al.*, 2004]; (2) fault-valve systems (e.g., inter-seismically impermeable fault transecting the suprahydrostatic pressure gradient [*Sibson*, 1992]); and (3) metamorphic dehydration in thrust and normal fault systems [*Walder and Nur*, 1984; *Wong et al.*, 1997; *Ague et al.*, 1998; *Seno*, 2005]. One of the likely mechanisms of triggering is the diffusive process of pore pressure relaxation in fractured and/or porous rock [e.g., *Healy et al.*, 1968; *Hsieh and Bredehoeft*, 1981; *Shapiro et al.*, 2003, 2006].

[3] Although the mechanics of fault slip reactivation due to a pore pressure perturbation has been extensively studied [*Hubbert and Rubey*, 1959; *Raleigh et al.*, 1976; *Scholz*, 1990; *Rice*, 1992], there is still a considerable lack of understanding of (1) fundamental conditions under which the reactivation of fault slip by elevated pore pressure leads to the nucleation of dynamic (earthquake) rupture, (2) the extent of dynamic rupture propagation before it is arrested, and (3) what separates micro-seismic events from earthquakes.

[4] We address these questions by analyzing a simplified model of nucleation and possible arrest of dynamic slip on a pressurized fault characterized by initially uniform frictional strength and loaded by uniform prestress (background stress field). An evolving, locally peaked pore pressure profile is generated by along-the-fault diffusion from a fluid source characterized by either constant overpressure or a constant flow rate. As a result, the frictional strength of the fault, given by the product of the local normal *effective* stress and slip-weakening friction coefficient [*Ida*, 1972; *Palmer and Rice*, 1973; *Rice*, 1980; *Wong*, 1986], diminishes below the background stress within the pressurized region, expanding with time. This causes

[1]Department of Civil and Resource Engineering, Dalhousie University, Halifax, Nova Scotia, Canada.
[2]School of Civil and Environmental Engineering, Georgia Institute of Technology, Atlanta, Georgia, USA.

Corresponding author: D. I. Garagash, Department of Civil and Resource Engineering, Dalhousie University, 1360 Barrington St., Halifax, NS B3J 1Z1, Canada. (garagash@dal.ca)

0148-0227/12/2012JB009209

a shear crack, with growth initially moderated by pressure diffusion and thus being quasi-static. The slip-weakening nature of friction suggests that quasi-static growth may eventually become unstable leading to the nucleation of dynamic rupture [*Campillo and Ionescu*, 1997; *Ionescu and Campillo*, 1999; *Uenishi and Rice*, 2003; *Rice and Uenishi*, 2010]. In this paper, we extend the approach of *Uenishi and Rice* [2003], who studied nucleation due to locally peaked *fault loading* under dry or drained fault conditions. We determine the extent of the nucleation patch and the time to nucleation due to local changes to the *fault strength* resulting from a pore pressure perturbation. A similar approach has been independently used by *Viesca and Rice* [2012] to analyze nucleation of dynamic submarine and subareal landsliding, and numerically implemented in simulations of seismicity caused by CO_2 geological sequestration by *Cappa and Rutqvist* [2011].

[5] In this first-order model we use a simple slip-dependent friction law in favor of a potentially more complete, laboratory-derived description [e.g., *Marone*, 1998] in which friction depends on slip rate and state. *Tse and Rice* [1986], *Dieterich* [1992], *Lapusta et al.* [2000], *Rubin and Ampuero* [2005], *Ampuero and Rubin* [2008], among others, studied earthquake nucleation for rate- and state- dependent friction laws. *Uenishi and Rice* [2003] suggested, in the context of nucleation of dynamic slip on a well-healed fault, that the linear slip-weakening law may provide an approximation of the rate- and state-dependent friction of ageing type [*Ruina*, 1983]. They cautioned that their conjecture may require unrealistic values of friction parameters. More recently, however, *Rubin and Ampuero* [2005] and *Ampuero and Rubin* [2008] identified two end-member length scales for the nucleation patch. The first end-member is identical to that obtained by *Dieterich* [1992] and *Uenishi and Rice* [2003] for the linear slip-weakening friction law. The second end-member can be linked (see section 7.1) to *Andrews*' [1976] critical length scale appearing from the slip-weakening friction law with constant stress-drop. This correspondence between the end-members obtained in the context of the rate- and state-dependent friction and for rate-independent slip-weakening lends some confidence in using the simplified slip-weakening friction framework to study earthquake nucleation.

[6] Other simplifying assumptions of this work include neglecting the effect of poroelastic changes of the background stress level [e.g., *Segall*, 1989; *Rudnicki*, 1999; *Germanovich and Chanpura*, 2002], as well as the effect of inelastic changes of gouge porosity and permeability with the slip [*Rice*, 1992; *Segall and Rice*, 1995; *Garagash and Rudnicki*, 2003, and references therein].

[7] The arrest of dynamic rupture is usually associated with the non-uniformity of prestress distribution and/or fault strength. Such non-uniformity can reflect, for example, finiteness of immature faults or pre-existing fractures, which results in a significantly elevated cohesive component of strength at the "tips", and geometrical complexities and the segmentation of mature faults [*Sibson*, 1986; *Scholz*, 1990]. Another possible rupture arrest mechanism, investigated further in this work, is related to the limited nature of the frictional weakening with increasing slip. This is expected to be a dominant mechanism if the rupture extent is smaller than the length scale of fault prestress/strength heterogeneity.

[8] In order to assess the run-out distance of a dynamic rupture before it is arrested, we analyze alternative quasi-static solutions for the slipping patch past the point of dynamic instability. This analysis suggests that the arrest of the dynamic rupture propagation is possible if the background loading on the fault is equal or less than the residual (weakened) fault strength at the ambient pore pressure. In this case, the dynamic rupture is nucleated from the slipping patch, which is embedded within the zone where the pore pressure is elevated by diffusion. The rupture is arrested as its front grows out to the margins of the pressurized zone. This situation is markedly different from the case where the fault state is initially close to failure (i.e., when the background stress is close to the peak fault strength at ambient conditions). Then the growth of the nucleated dynamic rupture is unabated within the constraints of the model developed in this work.

[9] We also consider a possibility that other, dynamic weakening processes (different from the "quasi-static" slip weakening during the nucleation stage) can be activated by fault frictional heating in the course of seismic slip. Depending on gouge properties and prevailing fault conditions, these weakening processes can include flash heating on asperities [*Rice*, 2006; *Beeler et al.*, 2008; *Rempel and Weaver*, 2008], thermal pressurization of pore fluid [*Sibson*, 1973; *Lachenbruch*, 1980; *Andrews*, 2002; *Garagash and Rudnicki*, 2003; *Bizzarri and Cocco*, 2006a; *Rice*, 2006; *Garagash*, 2012], and macroscopic melting or thermal decomposition reactions [e.g., *Rice*, 2006; *Di Toro et al.*, 2011, and references therein]. Recent studies of kinematic slip [*Rempel and Rice*, 2006] and pulse-like dynamic slip [*Garagash*, 2012] showed that thermal pressurization can effectively cap the temperature rise, and, in the case of a pulse-like rupture, all but rule out melting and some thermal decomposition reactions at seismogenic depth. Yet, the possibility of co-seismic melting does remain viable in the crack-like mode of rupture [e.g., *Bizzarri and Cocco*, 2006b]. In this work, we examine if the co-seismic flash heating or thermal pressurization can allow rupture propagation beyond the otherwise predicted arrest length. This would constitute a scenario of an earthquake nucleation on a statically strong but dynamically weak fault [*Lapusta and Rice*, 2003; *Rice*, 2006; *Noda et al.*, 2009; *Garagash*, 2012].

[10] Finally, we discuss possible implications of our results to patterns of seismicity induced by deep fluid injection and lower and upper bounds for microseismicity (determined, respectively, by minimum nucleation size and maximum run-out distance, which does not yet activate dynamic fault weakening processes). We also discuss a possible gap in magnitude between induced microseismic events and larger earthquakes [e.g., *Healy et al.*, 1968] and a possible change of the focal mechanism from smaller to larger events.

2. Equilibrium of a Slip-Weakening Fault

[11] We consider a mode II or III shear crack of length $2a = a_+ - a_-$ in the uniform background stress field characterized by the normal σ_n and shear τ^b components (Figure 1a). Shear stress τ on the fault plane is related to slip δ (shear displacement discontinuity) by the equation of quasi-static elastic equilibrium [e.g., *Bilby and Eshelby*, 1968]

$$\tau(x,t) - \tau^b = -\frac{\mu^*}{2\pi} \int_{a_-(t)}^{a_+(t)} \frac{\partial \delta(s,t)}{\partial s} \frac{ds}{x-s}, \qquad (1)$$

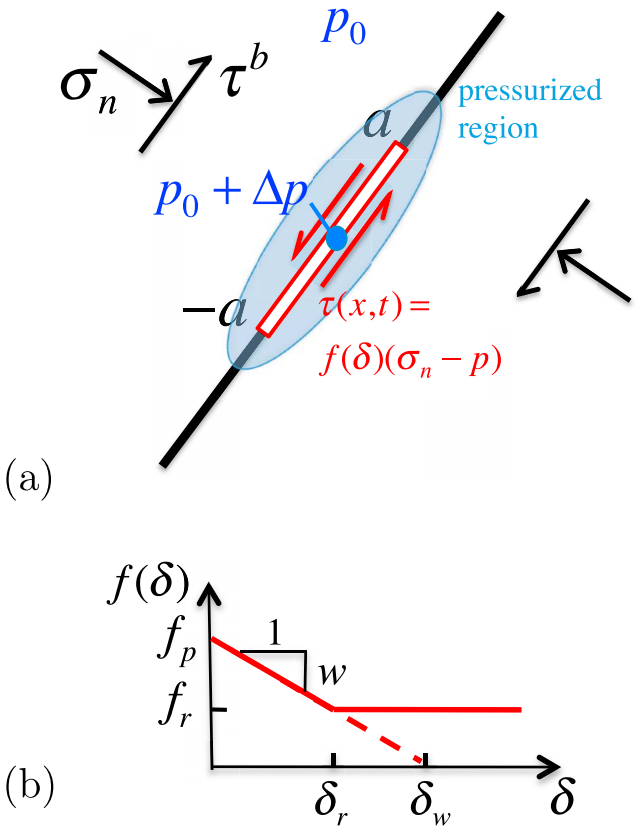

Figure 1. (a) A growing slip patch (shear crack) due to fluid injection into a uniformly loaded fault. (b) Linear slip weakening of fault friction $f(\delta)$ with (horizontal solid line) or without (inclined dashed line) residual cut-off .

where $\mu^* = \mu$ (shear modulus) for Mode III and $\mu^* = \mu/(1-\nu)$ (a half of the plane-strain modulus) for Mode II, ν is the Poisson's ratio. Slip rate $V = \partial\delta/\partial t$ vanishes at the crack tips, which imposes the following two constraints on the distribution of the shear traction $\tau(x, t)$ along the crack [*Rice*, 1968]:

$$\int_{a_-(t)}^{a_+(t)} \frac{\tau(x,t)-\tau^b}{\sqrt{a(t)^2-x^2}}dx = 0, \quad \int_{a_-(t)}^{a_+(t)} \frac{\tau(x,t)-\tau^b}{\sqrt{a(t)^2-x^2}}xdx = 0. \tag{2}$$

These two conditions also ensure that the stresses at the tip are bounded and continuous (i.e., vanishing tip stress intensity factors). In this work, we consider symmetric shear traction distributions, which imply that the crack is symmetric,

$$a_+ = -a_- = a, \tag{3}$$

and that the second constraint in (2) is automatically satisfied.

[12] Inside the slipping region, the shear stress is equal to the fault shear strength,

$$\tau = f(\delta)(\sigma_n - p), \tag{4}$$

where $\sigma_n - p$, also denoted as $\overline{\sigma}$, is the effective stress normal to the fault and the friction coefficient

$$f(\delta) = f_p - w\delta \qquad \left(0 \le \delta < f_p/w\right). \tag{5}$$

decreases linearly with the slip (Figure 1b) from its peak value f_p [e.g., *Ida*, 1972]. The implicit assumption associated with using the unlimited slip-weakening relation (5) is that during the nucleation process, the quasi-static slip is small enough, such that the corresponding reduced strength remains above the residual fault strength. This assumption is evaluated aposteriori, and the influence of the residual fault strength on the dynamic slip nucleation and its possible arrest is considered in section 5.

[13] Elastic equilibrium (1) and constitutive laws (4)–(5) can be used to describe quasi-static development of a slipping patch in response to a change of the background loading τ^b [*Uenishi and Rice*, 2003; *Dascalu et al.*, 2000] and/or change of the fault strength associated with the corresponding increase of pore pressure. The latter is the focus of this paper.

3. Fault Slip Due to Pore Pressure Loading

[14] Consider the no-slip initial conditions when the background shear stress τ^b is smaller than the ambient peak strength $\tau_p = f_p(\sigma_n - p_o)$, where p_o is the ambient pore pressure on the fault plane. A pore pressure perturbation Δp introduced at a given location $x = 0$ along the fault at $t \ge 0$ causes a reduction of the shear strength. This reduction is sufficient to activate the slip if

$$\tau^b \ge \tau_p - f_p \Delta p. \tag{6}$$

Spreading of the region with reduced fault strength by the pore pressure diffusion results in enlarging the slip zone.

[15] To illustrate this type of slip process, consider evolving pore pressure perturbation $p - p_o$ along the fault (Figure 1a) in the following form:

$$p(x,t) - p_o = \Delta p(t)\Pi(\xi), \quad \xi = x/\sqrt{\alpha t}, \tag{7}$$

where α is the hydraulic diffusivity $[L^2/T]$ and $\Pi(\xi)$ is a function describing instantaneous spatial profiles of the pressure perturbation. This is a general type of spatiotemporal distribution due, for example, to the pore pressure diffusion from a point (line) source in the fault plane [e.g., *Carslaw and Jaeger*, 1959]. Such a situation can be envisioned if a borehole is drilled along the fault plane (orthogonal cross-section of which is shown in Figure 1a) and fluid is injected into the borehole to trigger an earthquake in more controllable conditions than it would happen otherwise [*Garagash et al.*, 2009; *Germanovich et al.*, 2010, 2011]. Examples of the injection scenarios, for which the pressure along the fault is described by (7) include fluid injection into the fault zone characterized by negligible transverse permeability, under a constant overpressure Δp,

$$\Delta p(t) = const, \qquad \Pi(\xi) = \mathrm{Erfc}|\xi|, \tag{8}$$

or, at a constant flow rate q $[L/T]$,

$$\Delta p(t) = \frac{2}{\sqrt{\pi}}\frac{\eta q}{k}\sqrt{\alpha t}, \quad \Pi(\xi) = \exp\left(-\xi^2/4\right) - \frac{\sqrt{\pi}}{2}|\xi|\mathrm{Erfc}\frac{|\xi|}{2}, \tag{9}$$

where η is the fluid viscosity and k is the longitudinal permeability of the fault zone.

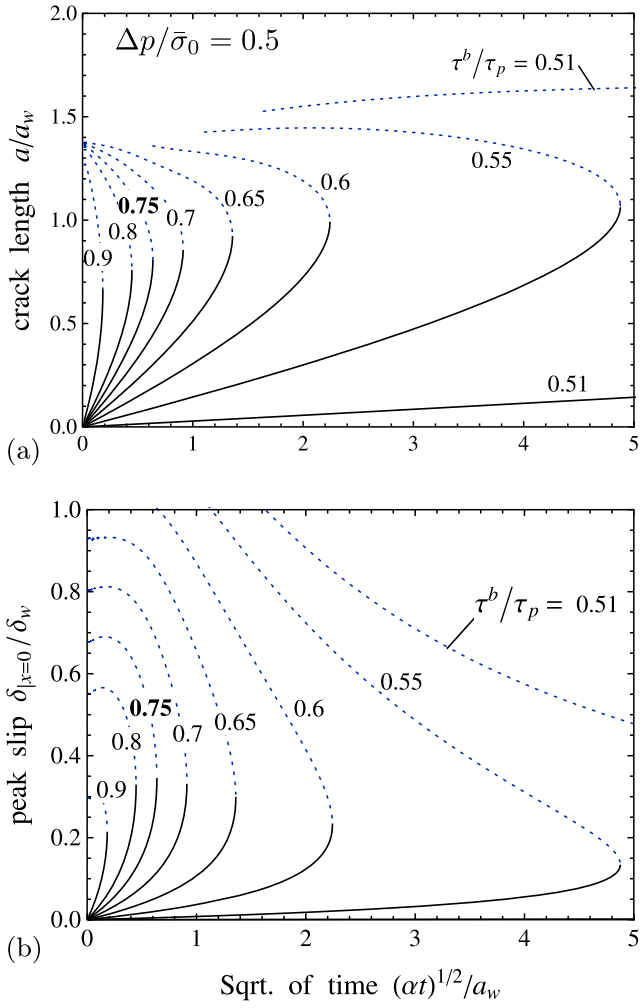

Figure 2. Development of (a) the crack half-length and (b) the slip at the crack center for the overpressure at the crack center $\Delta p/\bar{\sigma}_o = 0.5$ and various values of the background stress τ^b/τ_p. The rightmost points of each curve (i.e., with vertical slope) correspond to the instability of quasi-static crack growth. Beyond these points, continued quasi-static growth would require either reduction of the background stress or, conceivably, injection shut-in. Dotted parts of the curves correspond to the crack growth under physically *meaningless* reversal of the pore pressure diffusion (time reversal) at the fixed level of background stress.

[16] An example of pressure distribution more general than (7) is given by the point (line) injection into the rock, with isotropic permeability k_1, at distance L from the fault plane and at a constant rate Q [L^2/T]. For a permeable fault with permeability $k = k_1$,

$$\Delta p(t) = \frac{-\mathrm{Ei}\left(-\xi_L^2/4\right)}{2\pi^2}\frac{\eta Q}{k_1}, \quad \Pi(\xi,\xi_L) = \frac{\mathrm{Ei}\left(-\left(\xi^2+\xi_L^2\right)/4\right)}{\mathrm{Ei}\left(-\xi_L^2/4\right)}, \tag{10}$$

where $\xi_L = L/\sqrt{\alpha t}$ and Ei is the exponential integral [*Abramowitz and Stegun*, 1972]. In the case of an impermeable fault plane ($k = 0$), $\Delta p(t)$ in (10) has to be increased by the factor of two.

[17] Nondimensionalizing of the set of equations (1), (2), (3)–(5), and (7) suggests that the normalized slip δ/δ_w and the normalized half-length of the slipping patch (zone) a/a_w can be expressed in terms of the normalized coordinate $X = x/a$, normalized time $\alpha t/a_w^2$, and two dimensionless loading parameters, namely, fault understress $(\tau_p - \tau^b)/\tau_p$ and fluid overpressure $\Delta p/\bar{\sigma}_o$ ($\bar{\sigma}_o = \sigma_n - p_o$). Hereafter,

$$a_w = \frac{\mu^*}{\tau_p}\delta_w, \qquad \delta_w = \frac{f_p}{w} \tag{11}$$

are the characteristic patch length and slip weakening scale, respectively. In the case (10) of fluid injection at a distance from the fault plane, an additional parameter is the scaled distance, ξ_L. The numerical solution method, used to solve the nondimensionalized set of equations, relies on expansion of slip into a series of Chebyshev polynomials, which is presented in Appendix A.

[18] Development of slip due to the fluid injection with the constant value of overpressure, $\Delta p/\bar{\sigma}_o = 0.5$, into a fault zone characterized by negligible transverse permeability (equations (7) and (8)), can be seen in Figures 2 and 3. Figure 2

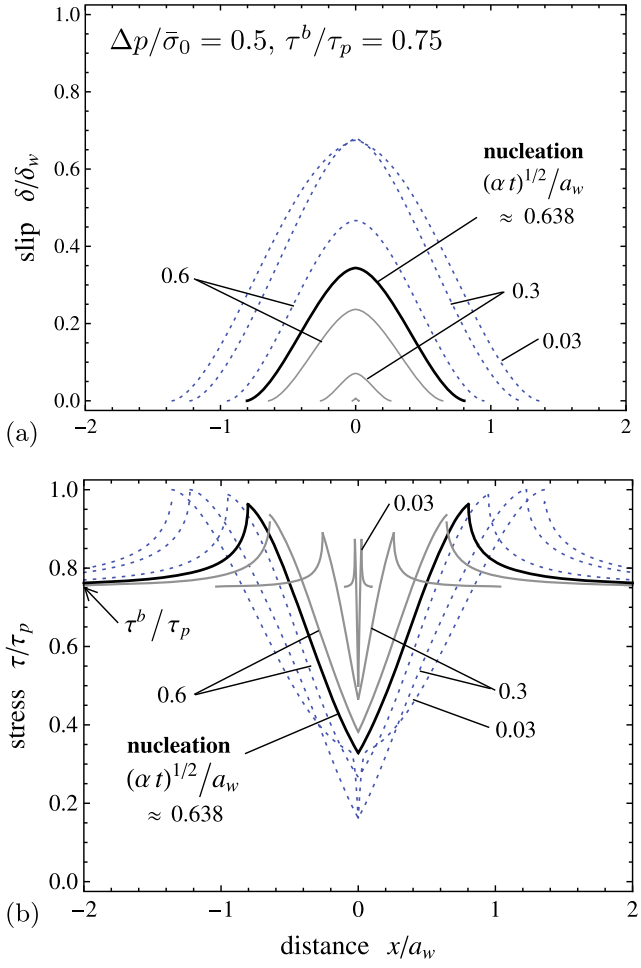

Figure 3. Development of (a) slip and (b) shear stress distributions for $\Delta p/\bar{\sigma}_o = 0.5$ and $\tau^b/\tau_p = 0.75$. The heavy line corresponds to the instability of the quasi-static slip growth under sustained injection of fluid at the crack center. Dotted lines correspond to a physically unrealistic solution depicted in Figure 2 (also by dotted lines).

shows evolution of the normalized crack half-length (Figure 2a) and the slip at the patch center $x = 0$ (Figure 2b) with advance of the pore pressure diffusion "front" (characterized by its normalized position $\sqrt{\alpha t}/a_w$) for various values of the normalized background stress τ^b/τ_p. Both time to instability (or nucleation time) and the corresponding critical length of the crack (or the length of the nucleation patch) correspond to the points with the vertical slope in Figure 2. Values of the nucleation time and length increase with decreasing background loading (Figure 2a), while the slip at the center reaches its maximum for the intermediate value of $\tau^b/\tau_p \simeq 0.75$ (Figure 2b). The dotted parts of the curves correspond to the crack growth under physically meaningless reversal of the pore pressure diffusion (time decrease). Therefore, after the slip zone reaches a critical size, quasi-static equations cannot describe its further development, which corresponds to the initiation of dynamic slip (earthquake nucleation). For smaller values of the background stress ($\tau^b/\tau_p \le 0.6$), dotted curves in Figures 2a and 2b are terminated when the fault frictional strength (equations (4)–(5)) is reduced to zero (dashed line in Figure 1b) at the center of the crack when $\delta_{|x=0} \to \delta_w$. Clearly, the frictional model with unconstrained slip-weakening (5) ought to be amended at the slip values $\gtrsim \delta_w$, for example, by introducing a non-zero residual friction. The effect of the residual friction on the dynamic slip nucleation and its possible arrest is discussed in section 5.

[19] Development of the slip and the shear stress distributions with the normalized position of the diffusion front is shown in Figures 3a and 3b, respectively, for the background stress of $\tau^b/\tau_p = 0.75$ and overpressure $\Delta p/\overline{\sigma}_o = 0.5$. Bold line corresponds to the instability of the quasi-static crack growth and nucleation of the dynamic slip. Stress profiles corresponding to small times are characterized by spikes near the fluid source (the crack center).

4. Conditions for Nucleating Dynamic Slip

[20] Differentiating (1) with respect to time and accounting for (4) and (5), we obtain equation

$$wV(x,t)\overline{\sigma}(x,t) - f(\delta(x,t))\frac{\partial \overline{\sigma}(x,t)}{\partial t} + \frac{\partial \tau^b(x,t)}{\partial t} = = \frac{\mu^*}{2\pi}\int_{-a(t)}^{a(t)} \frac{\partial V(s,t)}{\partial s}\frac{ds}{x-s} \qquad (12)$$

governing the slip rate distribution $V = \partial\delta/\partial t$ along the crack, $|x| < a(t)$. The instability of quasi-static crack growth, as illustrated in section 3, corresponds to the diverging rate of slip. Let t_c be the nucleation time and $a_c = a(t_c)$ the half-length of the nucleation patch. As the instability is approached when $t \to t_c$, the bounded terms $f\partial\overline{\sigma}/\partial t$ and $\partial\tau^b/\partial t$ in (12) become negligible when compared to the remaining diverging terms. Slip velocity, normalized by its root-mean-square, can be written as a function of the normalized coordinate $X = x/a(t)$:

$$v(X,t) = \frac{V(a(t)X,t)}{\sqrt{\frac{1}{2}\int_{-1}^{1} V^2(a(t)X,t)dX}}. \qquad (13)$$

At the time of nucleation, $t = t_c$, (12) can be then written as

$$\frac{a}{a_w}v(X)\frac{\overline{\sigma}(aX)}{\overline{\sigma}_o} = \frac{1}{2\pi}\int_{-1}^{1}\frac{dv(s)}{ds}\frac{ds}{X-s}. \qquad (14)$$

[21] When the effective normal stress $\overline{\sigma}(x)$ is known along the slipping patch, (14) is a linear homogeneous equation for the normalized slip rate distribution $v(X)$. This equation has a non-zero solution only for values of the normalized nucleation half-length a/a_w that correspond to eigenvalues of problem (14). In the particular case of the uniform distribution of the normal effective stress along the crack ($\overline{\sigma}(x) = \overline{\sigma} = \text{const}$), (14) has been solved by *Uenishi and Rice* [2003], with the smallest eigenvalue, which corresponds to the nucleation half-length, given by

$$\frac{a_c}{a_w} \simeq 0.579\frac{\overline{\sigma}_o}{\overline{\sigma}} \quad (\overline{\sigma} = \text{const}). \qquad (15)$$

[22] In the case of the pore pressure loading (7) due to fluid injection into the fault, we have

$$\overline{\sigma}(aX) = \overline{\sigma}_o - \Delta p(t)\Pi\left(aX/\sqrt{\alpha t}\right),$$

and the solution of (14) for the normalized half-length a_c/a_w of the nucleation patch depends upon two parameters: the normalized overpressure $\Delta p(t_c)/\overline{\sigma}_o$ at the crack center and the normalized square root of the nucleation time $\sqrt{\alpha t_c}/a_w$ (or normalized position of the pressure diffusion "front"). The corresponding magnitude of the background shear stress, required to reach nucleation, cannot be recovered from the solution of the eigenvalue problem (14), and requires solving the full set of slip equations (1)–(7) at the nucleation instant (i.e., at $t = t_c$ and $a = a_c$ for a given value of the overpressure $\Delta p(t_c)$ at the patch center $X = 0$).

[23] Let us first consider two limiting cases when at the nucleation time, the slip zone is much larger or much smaller than the pressure diffusion scale in the fault zone. As discussed below, a "large" slip zone, $a_c \gg \sqrt{\alpha t_c}$, is expected in critically loaded faults, which are stressed almost to their strength level ($\tau_p - \tau^b \ll f_p\Delta p$). A "small" slip zone, $a_c \ll \sqrt{\alpha t_c}$, would appear in faults that are pressurized merely enough to activate the fault slip ($\tau_p - \tau^b \simeq f_p\Delta p$) and only at the slip zone center, where the pressure is the largest. In these limiting cases, the solution at the instability can be established for a general pressurization scenario, not constrained to a specific form of the pressurization function $\Pi(\xi)$ in (7).

4.1. Nucleation on a Marginally Pressurized Fault ($f_p\Delta p \simeq \tau_p - \tau^b$)

[24] In this case, a localized pore pressure increment Δp is just enough to activate the fault slip near $x = 0$. The subsequent quasi-static growth of the slipping patch will be much slower than the diffusive growth of the pressurized zone. As a result, at the instability, the crack will be well within the pressurized region ($a_c \ll \sqrt{\alpha t_c}$), and, therefore, will be almost uniformly pressurized, so that $p(x, t_c) \simeq p_o + \Delta p$ for

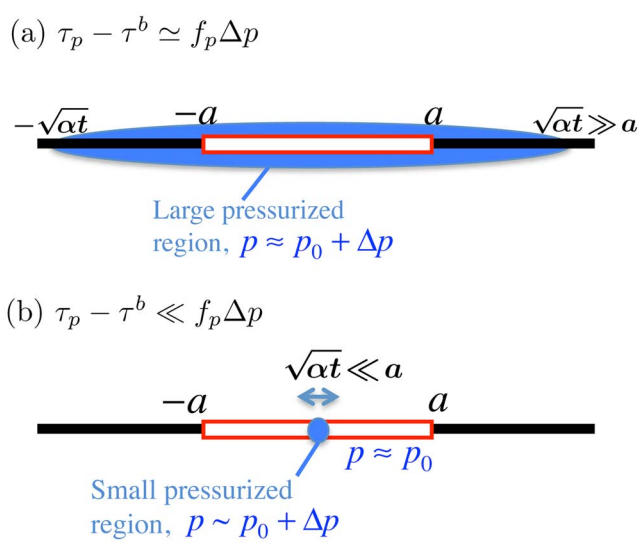

Figure 4. Two limiting responses of a fault to pressurization: (a) marginally pressurized fault ($f_p\Delta p \simeq \tau_p - \tau^b$), and (b) critically loaded fault ($\tau^b \simeq \tau_p$).

$|x| \le a_c$ (Figure 4a). Consequently, an asymptotic expression for the nucleation length follows from (15) in the form of

$$\frac{a_c}{a_w} \simeq 0.579 \frac{\tau_p}{\tau^b}, \tag{16}$$

where the limit value $(\tau_p - \tau^b)/f_p$ of overpressure Δp has been used to evaluate $\overline{\sigma} \approx \overline{\sigma}_0 + \Delta p$ in (15). Expression (16) gives the smallest possible nucleation length (corresponding to the smallest Δp required to activate the slip) for a given fault background loading τ^b. The asymptotic solution developed in Appendix B suggests the scaling

$$\frac{\delta}{\delta_w} \sim \frac{f_p \Delta p(t) - (\tau_p - \tau^b)}{\tau^b} \qquad (\delta \ll \delta_w)$$

for the fault slip. The corresponding distribution $\delta(x, t_c)$ is shown in Figure 5 for the case of linear (injection into transversely impermeable fault) and radial (injection into the rock with isotropic permeability) diffusions. Note that in this work, we use symbols $\sim$ and O of asymptotic order interchangeably.

[25] The respective solution for the nucleation time depends on the injection scenario. For example, in the case of fluid injection into a transversely impermeable fault at a constant injection pressure (equations (7) and (8)), the nucleation time can be recovered from equations (B4a) and (B5a) (Appendix B):

$$\frac{\sqrt{\alpha t_c}}{a_c} \simeq 0.454 \left(1 - \frac{\tau_p - \tau^b}{f_p \Delta p}\right)^{-1}. \tag{17}$$

[26] For injection at a constant injection rate $q = const$, expression (9a) for the overpressure evolution can be alternatively written as

$$\frac{\Delta p(t)}{(\Delta p)_w} = \frac{\sqrt{\alpha t}}{a_w}, \qquad (\Delta p)_w = \frac{2}{\sqrt{\pi}} \frac{\eta}{k} q a_w \qquad (q = const) \tag{18}$$

where $(\Delta p)_w$ is a characteristic pressure drop over distance a_w from the crack center. Then, the expression for the time of nucleation

$$\frac{\sqrt{\alpha t_c}}{a_w} \simeq \frac{\tau_p - \tau^b}{f_p (\Delta p)_w} \tag{19}$$

follows from setting $\Delta p(t_c)$ in (18) to the value of $(\tau_p - \tau^b)/f_p$ at the slip activation, on the premise that in this case, the instability follows shortly after the activation. This assumption is valid for slow injection rates ($q \ll (\tau_p - \tau^b)\sqrt{\pi}k/(2\eta a_w)$), when the characteristic pressure drop $(\Delta p)_w$ is small compared to $\Delta p(t_c) \simeq (\tau_p - \tau^b)/f_p$.

[27] When the fluid is injected at a distance L from the fault plane into a rock with isotropic permeability, the nucleation time can be found in a similar fashion by approximating the nucleation time by the slip activation time, setting $\Delta p(t_c) = (\tau_p - \tau^b)/f_p$ in (10a), and solving the resulting implicit equation for $L/\sqrt{\alpha t_c}$. This approximation is permissible if the distance of the injection point from the fault is much larger than the crack length ($\sim a_w$) at the instability, i.e., if $L \gg a_w$.

[28] Finally, it is worth stressing that because $f_p\Delta p \simeq \tau_p - \tau^b$, the normalized slip at nucleation is small ($\delta/\delta_w \ll 1$) while the normalized nucleation time is large ($\sqrt{\alpha t_c}/a_w \gg 1$). That the slip is small ($\delta \ll \delta_w$) is consistent with the fact that we neglected the cut-off part of the slip weakening friction law (solid horizontal line in Figure 1b). Hence, for marginally pressurized faults with a small slip zone ($a_c \ll \sqrt{\alpha t}$), the residual friction is likely not achieved by the moment of dynamic slip nucleation.

4.2. Nucleation on a Critically Loaded Fault ($\tau^b \simeq \tau_b$)

[29] A fault that is stressed almost to its static strength level requires only a small stress or strength perturbation to reach the instability. In the context of this paper, a small strength perturbation is achieved by finite pore pressure

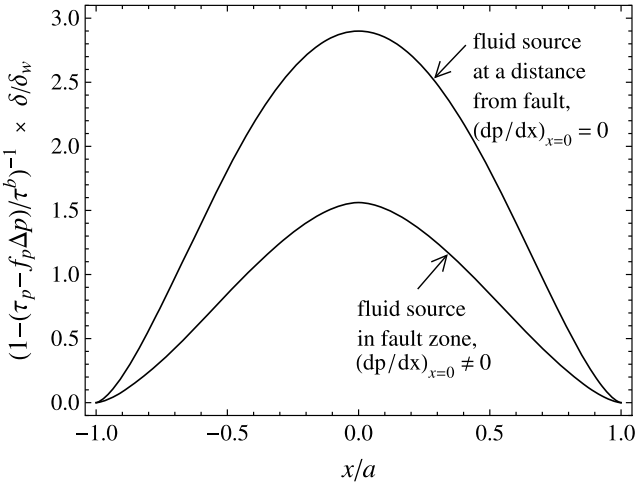

Figure 5. Asymptotic solutions for the slip $\delta(x, t_c)$ on a marginally pressurized fault ($f_p\Delta p(t_c) \simeq \tau_p - \tau^b$) at the instability for two pressurization scenarios corresponding to a fluid source in the fault zone (e.g., equations (8) and (9)) and at a distance from it (e.g., equation (10)). Fluid flow is symmetric about $x = 0$.

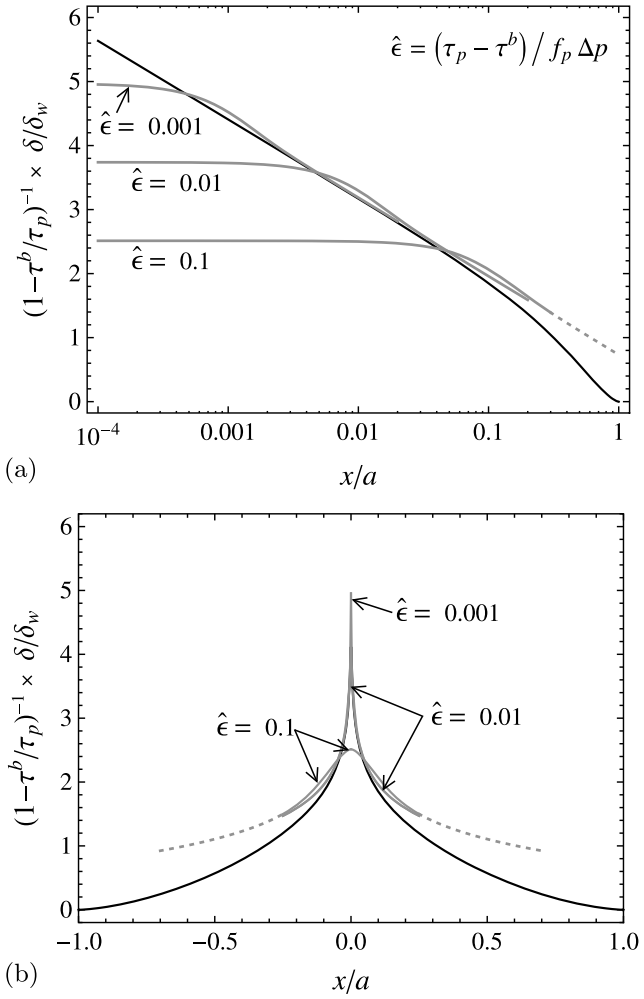

Figure 6. Asymptotic solution for slip on a critically loaded fault ($\tau^b \simeq \tau_p$) at the instability: the outer solution (black) at $x \gg \sqrt{\alpha t_c}$ and the inner solution (gray line, the case (8) of injection in transversely impermeable fault under constant injection pressure) at $x \sim \sqrt{\alpha t_c}$. The inner solution is shown for various values of the small parameter, $\hat{\epsilon} = (\tau_p - \tau^b)/(f_p \Delta p) \ll 1$, in (a) semi-logarithmic and (b) linear scale. The two solutions match at the intermediate length scale $\sqrt{\alpha t_c} \ll x \ll a_c$ near the crack center, where $\sqrt{\alpha t_c}/a_w \simeq 0.742\hat{\epsilon}$ and $a_c/a_w \simeq 0.579$.

increase Δp at the center of the crack over small injection times, such that at the instability, the size of the pressurized region is small compared to the size of the quasi-statically slipped crack, $\sqrt{\alpha t_c} \ll a_c$ (Figure 4b). As a result, the pressure is largely unperturbed (uniform) along the crack with the exception of the small pressurized "island" at the center. The corresponding asymptotic solution

$$\frac{a_c}{a_w} \simeq 0.579 \tag{20}$$

for the critical length of the quasi-static crack follows from (15) and $\overline{\sigma} \approx \overline{\sigma}_0$. Asymptotics outside of the small central region with perturbed pore pressure (outer solution) and inside that region (inner solution) are developed in Appendix C. At the instability, the integrated net overpressure (force) along the fault is

$$\Delta P(t_c) = \int_{-\infty}^{\infty} (p(x, t_c) - p_o) dx \simeq 0.837 \frac{\tau_p - \tau^b}{f_p} a_w, \tag{21}$$

which allows determining the nucleation time for a particular pressurization scenario. For example, in the case of injection into transversely impermeable fault zone, using (8) and (9) evaluates $\Delta P(t_c)$ to $(2/\sqrt{\pi})\Delta p \sqrt{\alpha t_c}$ ($\Delta p = const$) and $\sqrt{\pi}(\Delta p)_w \alpha t_c / a_w$ ($q = const$), respectively. The corresponding asymptotic solutions for the nucleation time follow from (21) as

$$\frac{\sqrt{\alpha t_c}}{a_w} \simeq \begin{cases} 0.742 \dfrac{\tau_p - \tau^b}{f_p \Delta p} & (\Delta p = const) \\ 0.687 \left(\dfrac{\tau_p - \tau^b}{f_p (\Delta p)_w} \right)^{1/2} & (q = const) \end{cases} \tag{22}$$

where $(\Delta p)_w$ is defined in (18).

[30] The outer solution suggests that the normalized slip scales with the understress when the latter is small, i.e., $\delta/\delta_w \sim (\tau_p - \tau^b)/\tau_p$ when $\tau_p - \tau^b \ll \tau_p$. The corresponding scaled slip distribution is universal (independent of a particular pressure profile) and shown in Figure 6 (solid line). In contrast, the inner solution for the slip inside the small pressurized region does depend on the pressure distribution (Appendix C). It is presented in Figure 6 by gray lines for the case of injection into a transversely impermeable fault at constant overpressure Δp (equations (7) and (8)), and three small values of parameter $\hat{\epsilon} = (\tau_p - \tau^b)/(f_p \Delta p)$, which is the understress normalized by the peak strength reduction. When $\hat{\epsilon} \ll 1$, the inner and outer slip solutions match at an intermediate distance, $0.742\hat{\epsilon} \ll x/a_w \ll 0.579$, from the crack center (Figure 6).

[31] The asymptotic expression for the peak slip $(\delta_{|x=0})_c$ at the instability follows from (C18) and can be written in a compact form upon relating Δp in parameter $\hat{\epsilon}$ at the nucleation to the nucleation time (22). As a result, we obtain

$$\frac{(\delta_{|x=0})_c}{\delta_w} \simeq \frac{\tau_p - \tau^b}{\tau_p} \left[-0.533 \ln \left(\frac{\sqrt{\alpha t_c}}{a_w} \right) + B \right] \tag{23}$$

where $B \simeq 1.127$ ($\Delta p = const$) and 0.860 ($q = const$).

4.3. Numerical Solution at the Instability

[32] Consider first injection into the transversely impermeable fault zone at constant injection pressure. Per (7) and (8) in this injection scenario, the effective normal stress along the fault is $\overline{\sigma}(x) = \overline{\sigma}_0 - \Delta p \Pi(\xi)$ with $\Pi(\xi) = \mathrm{Erfc}\,|\xi|$. In general, the solution of the linear eigenvalue equation (14) for the normalized nucleation half-length a_c/a_w and the normalized slip rate distribution $v(X)$, expressed as a function of $\Delta p/\overline{\sigma}_0$ and $\sqrt{\alpha t_c}/a_w$, does not explicitly depend on the background stress and its spatial distribution. As discussed later in this section, to determine the background stress magnitude for a given spatial profile, one needs to solve the full problem, (1)–(7), not just its eigenvalue reduction. In the meantime, we use the method of Chebyshev polynomial representation (section A1) to solve (14). Figure 7 illustrates

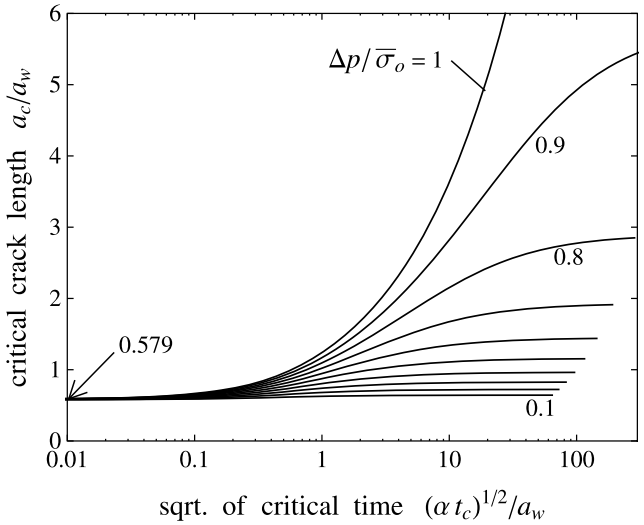

Figure 7. Solution of the eigenvalue problem (14) in the case of constant overpressure (Δp = const). Normalized crack half-length a_c/a_w is shown as a function of the square root of the normalized time to instability $\sqrt{\alpha t_c}/a_w$ and normalized overpressure $\Delta p/\overline{\sigma}_o$. This nucleation relationship (a_c vs. t_c and Δp) is applicable to an arbitrary spatial profile of the background stress. Its magnitude τ^b is uniquely determined from the solution of the full problem, (1)–(7), at the instability (see Figures 8a, 8c, and 8e for a uniform background stress profile).

the solution for the nucleation length for various values of the overpressure and the time to instability. The maximum overpressure value that we use, $\Delta p/\overline{\sigma}_o = 1$, corresponds to the complete loss of frictional strength at the injection point and possible onset of the along-the-fault hydraulic fracture. Note that because $\overline{\sigma}_o$ is, generally, not the least effective normal stress, it is also possible that hydraulic fracture may be initiated and propagated off the fault plane for Δp less than $\overline{\sigma}_o$. It can be seen in Figure 7 that the *Uenishi and Rice* [2003] value (20) of the normalized nucleation length is recovered for small nucleation times (i.e., when the pore pressure perturbation is localized near the crack center), which, as shown in this section, is synonymous to a critically loaded fault.

[33] The value of the uniform background stress τ^b required to reach the instability is recovered from the numerical solution of the full set of equations (1)–(7) (section A1) at the nucleation instant, characterized by the normalized critical crack length a_c/a_w given in Figure 7. This value allows us to recast the critical crack half-length and the nucleation time in terms of the two loading parameters, the fault understress $(\tau_p - \tau^b)/\tau_p$ and the fluid overpressure $\Delta p/\overline{\sigma}_o$ (Figures 8a and 8c). The corresponding slip at the crack center is shown in Figure 8e. For a given value of the overpressure, the solution exists in the range of background loading conditions, $0 < (\tau_p - \tau^b)/\tau_p \le \Delta p/\overline{\sigma}_o$, where the lower and upper bounds of the understress $\tau_p - \tau^b$ correspond to the asymptotics of the critically loaded and marginally pressurized faults, respectively. As already discussed, and further supported by the numerical solution, these asymptotic cases are characterized by the vanishing slip (Figure 8e) and the extreme values of the nucleation time. The latter vanishes for the low end and diverges for the high end values of the understress. To emphasize the relation of the general solution and its asymptotics, the solution for the critical crack half-length, the square root of the nucleation time, and the corresponding peak slip are recast in Figure S1 in the auxiliary material, in the scaling of a marginally pressurized fault.[1]

[34] The prominent feature of Figure 8a and its scaled representation, Figure S1a in the auxiliary material, is the weak dependence of the nucleation length on the fluid pressure. In other words, the nucleation length is largely controlled by the proximity of the fault loading to the static strength, quantified by the understress parameter $(\tau_p - \tau^b)/\tau_p$. The minimum nucleation length for a given background loading is given by the asymptote of the marginally pressurized fault,

$$\min(a_c/a_w) \simeq 0.579\left(\tau_p/\tau^b\right), \tag{24}$$

corresponding to the minimum value of pressure required to activate the slip. The maximum nucleation length is constrained by the value of the overpressure that would cause an incipient fault opening (hydraulic fracture) and the local loss of shear strength. It can be approximated (with < 1% error) by a two term expression

$$\max(a_c/a_w) \simeq 0.682\left(\tau_p/\tau^b\right) - 0.103\left(\tau^b/\tau_p\right). \tag{25}$$

[35] Change of the pressure boundary condition at the fluid source from a constant overpressure (equation (8)) to a constant fluid flux condition (equation (9)) leaves the nucleation length, including its minimum (24) and maximum (25) values, and critical slip predictions practically unchanged. This follows from comparing Figures 8a and 8b for the nucleation length, and Figures 8e and 8f for the slip. In the latter case, the two solutions are compared at the same values of the overpressure (dashed contour lines in Figure 8f). Two solutions for the nucleation time are qualitatively similar, but quantitatively different (solid lines in Figure 8c and dashed contour lines in Figure 8d), with shorter time to instability in the case of a constant fluid flux. Note that this quantitative difference is somewhat obscured by the semi-logarithmic scale of the Figures 8c and 8d.

[36] Although the numerical solutions at instability reported here are limited to two particular injection scenarios, Figure S1 in the auxiliary material suggests that accurate order-of-magnitude estimates of the nucleation length, time, and peak slip, can be obtained for a different injection scenario by interpolating between the two analytical asymptotes.

5. Effect of Residual Friction on Nucleation and Arrest of Dynamic Slip

[37] So far, the nucleation of the dynamic slip propagation due to the fault pressurization has been addressed in terms of the ideal linear slip-weakening of the fault friction (dashed line in Figure 1b). Physical extent of this weakening (at least under quasi-static slip conditions) is limited. That is, the friction is more likely to reach, eventually, a finite residual value at a large enough slip. Related questions are: (1) Can the limited

[1] Auxiliary materials are available in the HTML. doi:10.1029/2012GC004192.

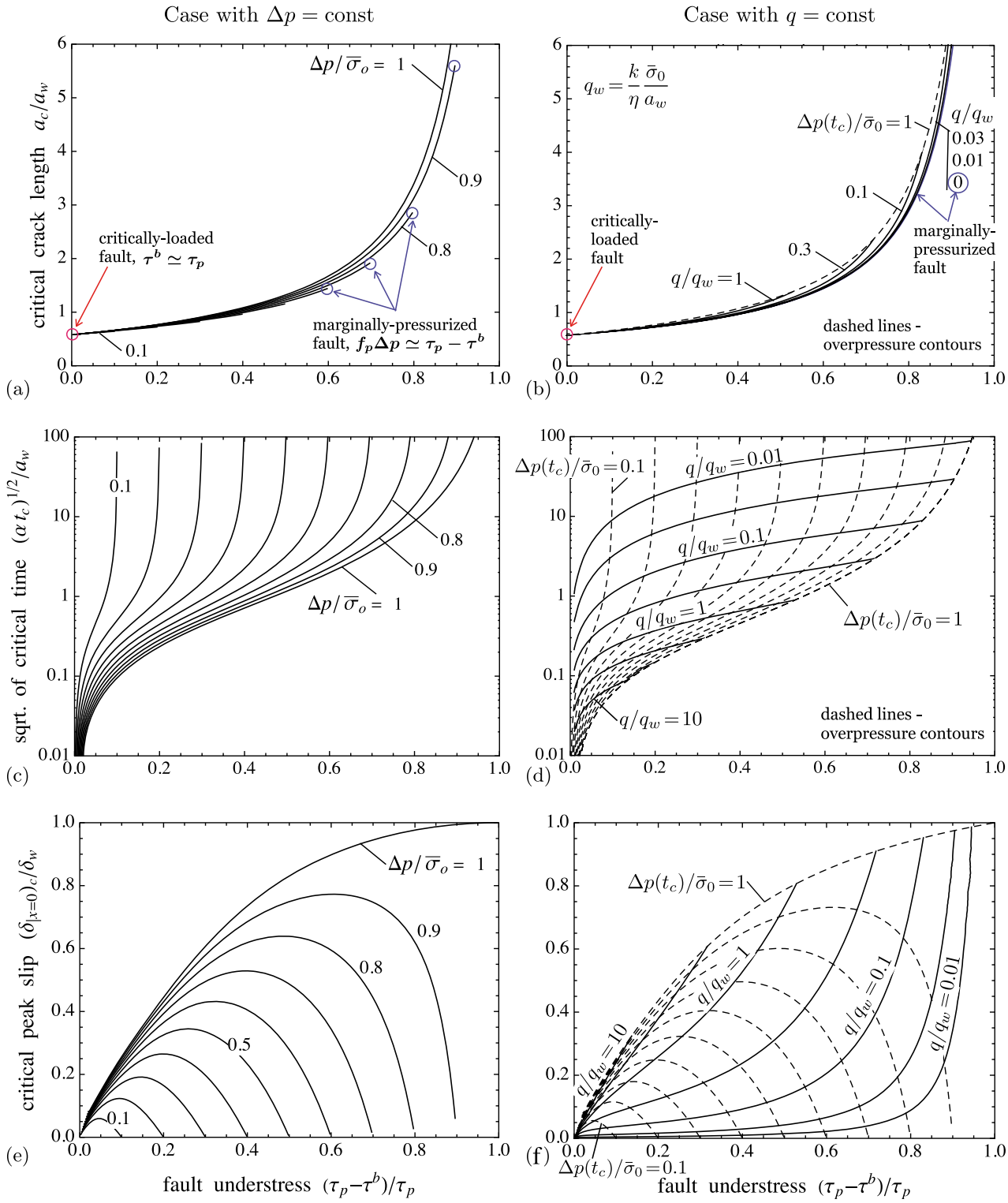

Figure 8. (a–b) Normalized crack half-length, (c–d) square root of time, and (e–f) slip at the crack center at the instability as functions of the fault understress $(\tau_p - \tau^b)/\tau_p$ for various constant values of the prescribed fluid overpressure $\Delta p/\bar{\sigma}_o$ (left) and injection rate q/q_w (right), where $q_w = (k/\eta)(\bar{\sigma}_0/a_w)$ is a characteristic flow rate. In the case of constant injection rate, the contour lines of the overpressure at nucleation, $\Delta p(t_c)/\bar{\sigma}_0 = (2/\sqrt{\pi})(q/q_w)(\sqrt{\alpha t_c}/a_w)$, are shown by dashed lines (right). The nucleation crack length (Figures 8a and 8b) and critical slip (Figures 8e and 8f) for two injection scenarios ((8) and (9)) are very close, while the sufficiently larger nucleation time is required in the case of constant overpressure (i.e., the dashed lines in Figure 8d are lower than the solid lines in Figure 8c, which is somewhat obscured by the semi-logarithmic scale).

nature of the fault friction weakening alter or suppress the dynamic instability? (2) Can it arrest otherwise dynamic rupture propagation? In this section, these questions are addressed by examining changes to the states of quasi-static crack equilibrium when the friction law (5) is amended by postulating that the friction slip-weakening is limited to the residual value, f_r, reached at the slip value of $\delta_r = (f_p - f_r)/w$:

$$f(\delta) = \begin{cases} f_p - w\delta, & \delta \le \delta_r \\ f_r, & \delta > \delta_r \end{cases} \tag{26}$$

[38] In relation to the first question, we note that since the slip on critically loaded ($\tau_p - \tau^b \ll f_p\Delta p$) or marginally pressurized ($\tau_p - \tau^b \simeq f_p\Delta p$) faults at the instability is small, the nucleation of dynamic slip for such faults is not affected by the limited slip-weakening. Further, examination of Figure 8e suggests that the peak slip at the instability $(\delta_{|x=0})_c$ in the model without residual friction may reach the minimum value $\delta_r = (1 - f_r/f_p)\delta_w$ at which the residual friction is probed only if the overpressure is large enough and the understress is within an intermediate subset from the range of $0 < \tau_p - \tau^b < f_p\Delta p$. For example, taking a representative value $f_r/f_p = 0.6$ (discussed in section 7.2) results in $\delta_r/\delta_w = 0.4$, and $\Delta p/\overline{\sigma}_o \gtrsim 0.6$ (more precisely $\gtrsim$0.565) is required to reach the residual friction level prior to the instability for these intermediate values of the understress (Figure 8e).

5.1. Numerical Examples

[39] Solution of the scaled set of equations (1)–(4), (26) and (7) for the normalized crack half-length a/a_w and slip δ/δ_w is a function of normalized time $\alpha t/a_w^2$, understress $(\tau_p - \tau^b)/\tau_p$, overpressure $\Delta p/\overline{\sigma}_o$, and the ratio of the residual to the peak friction coefficients, f_r/f_p. Since the slip-weakening region may no longer extend over the entire slip zone, resulting in a non-smooth stress distribution along it, the problem is more conveniently treated numerically by the piecewise constant displacement discontinuity (DD) method, as outlined in section A2.

[40] The development of the quasi-static crack (the crack length and the peak slip at the crack center) due to the pressurization of a slip-weakening fault with residual friction $f_r/f_p = 0.6$ is examined in Figure 9 for three values of the overpressure and various values of the understress $(\tau_p - \tau^b)/\tau_p$ from the corresponding ranges of $(0, \Delta p/\overline{\sigma}_o)$. Dotted lines show the solution for the model with unlimited slip weakening. Solutions for these two fault friction models are identical for $\delta \le \delta_r$ (e.g., compare Figure 9b to Figure 2 for $\Delta p/\overline{\sigma}_o = 0.5$). If the peak slip (at the crack center) exceeds the threshold of δ_r, a different path of the crack evolution before and after the initial instability can be realized.

[41] In the case of a small overpressure and the corresponding range of large background stress values (Figure 9a), the slip accumulated during the quasi-static growth of the crack to the instability is small, and, as anticipated, the nucleation of dynamic rupture ($da/dt \to \infty$) is not affected by the residual friction. Furthermore, there exist no quasi-static crack states with $a > a_c$, suggesting that the dynamic rupture propagation is unabated, at least, within the confines of the model of a homogeneous fault loaded by a uniform background stress.

[42] In the case of a moderate overpressure (Figure 9b), the initial instability is still unaffected by the residual friction, i.e., the peak slip at the instability is smaller than the residual value. However, different scenarios of the development of ensuing dynamic rupture can be forecasted based on the level of the background loading. For example, consider a possible path for the crack evolution with $\tau^b/\tau_p = 0.55$, as shown by arrows in Figure 9b. The crack growth occurs in three distinct episodes: (1) quasi-static crack development toward the initial point of instability A, (2) dynamic slip episode arrested at point B, and (3) subsequent quasi-static expansion of the slip zone. A necessary condition for the transition from the dynamic propagation back to the quasi-static one is linked to the existence of alternative quasi-static solution branches (for given fixed values of the background stress and overpressure) characterized by the increasing crack length with time. We observe that no such alternative branches exist for relatively large background stress ($\tau^b/\tau_p \gtrsim 0.74$ in Figure 9b), when the fault is relatively close to failure even prior to the pressurization. In this case, the limited amount of slip-weakening is sufficient to drive dynamic rupture without further pressurization. For smaller values of the background stress ($0.5 < \tau^b/\tau_p \le 0.6$), approaching the minimum set by the overpressure value, the pressurization is essential to drive the dynamic crack growth. Indeed, the transition from the dynamic slip (nucleated when the crack tips were well behind the pressure diffusion front $\sqrt{\alpha t}$) to the second quasi-static slip episode takes place when the crack tip "catches up" with the pressure diffusion "front". For intermediate values of the background stress ($0.6 < \tau^b/\tau_p < 0.74$ in Figure 9b), the crack evolution has two instability episodes: the first dynamic slip is arrested and followed by the intermediate period of quasi-static slip, which eventually leads to the re-nucleation and sustained propagation of the dynamic rupture. The evolution of stress and slip profiles for these three types of solution trajectories is controlled by the level of the background stress and illustrated in Figure S2 in the auxiliary material.

[43] Finally, in the case of large overpressure (Figure 9c), the development of slip is qualitatively similar to the previous case of a moderate overpressure for large and small values of the background stress, when the initial instability is not affected by the limited nature of fault-weakening. Namely, large background stress corresponds to a near-critical fault (e.g., $\tau^b/\tau_p = 0.8$) when the propagation of the dynamic rupture is unrestricted. In contrast, small background stress corresponds to a marginally pressurized fault (e.g., $\tau^b/\tau_p = 0.3$) when dynamic rupture is arrested. Different types of fault slip development are observed in the intermediate loading range ($0.36 \lesssim \tau^b/\tau_p < 0.8$), where the initial slip instability is altered by the limited friction weakening. In the ultimately stable part of this range ($0.36 \lesssim \tau^b/\tau_p \le 0.6$) the instability is suppressed completely, as a higher level of the quasi-static slip, compounded by lower background stress, results in the stabilization of the fault strength (at the residual value) before the instability can develop. In the ultimately unstable part of this stress range ($0.6 < \tau^b/\tau_p < 0.8$), the instability takes place at a larger quasi-static crack length than otherwise predicted in the model without the residual friction, and ensuing dynamic rupture propagation is unrestricted.

[44] We note that the existence of the alternative quasi-static crack solutions associated with the arrest of dynamic

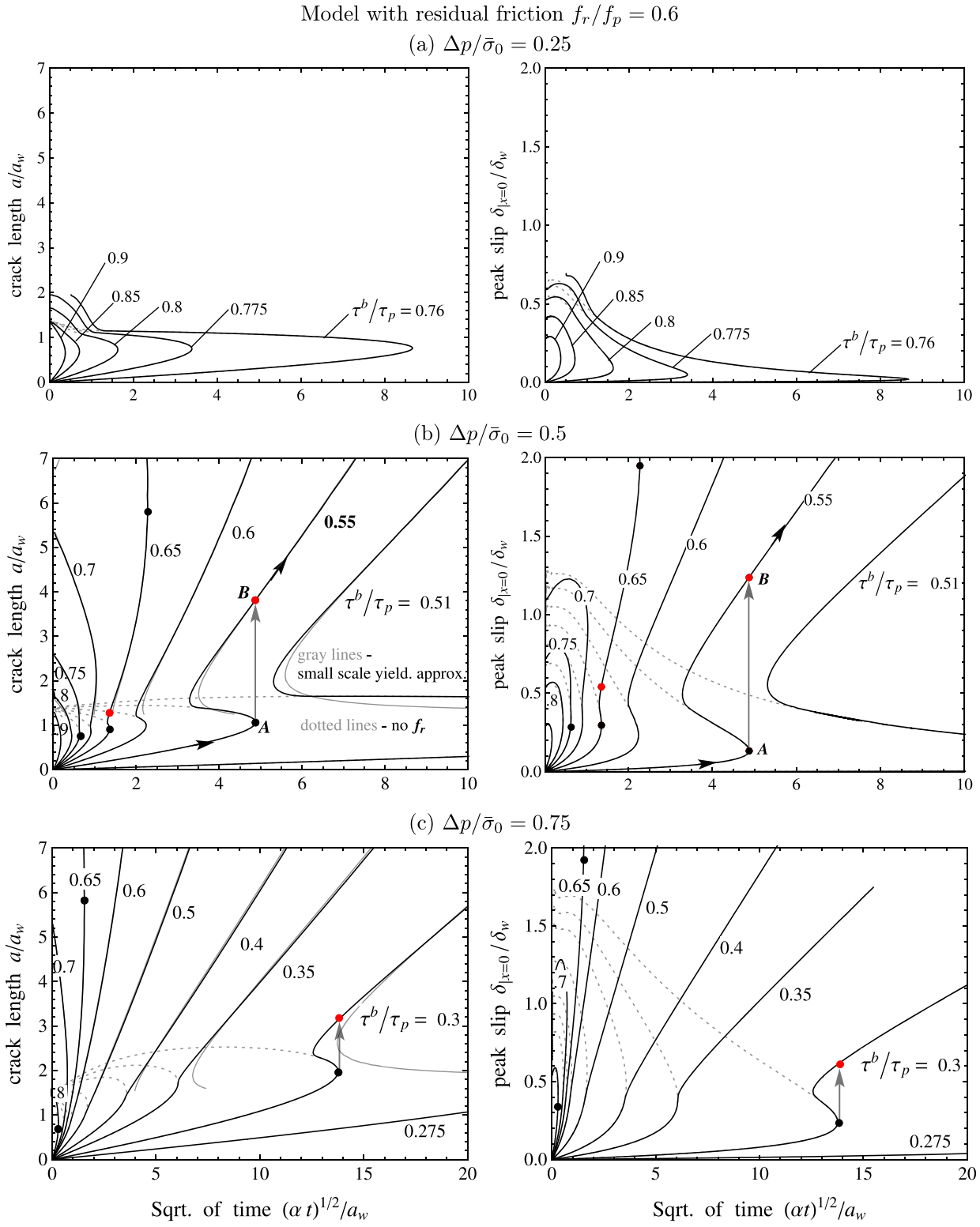

Figure 9. Development of (left) the normalized crack half-length and (right) the slip at the crack center for various values of the normalized fault background stress τ^b/τ_p and three values of the fixed overpressure at the center: (a) $\Delta p/\bar{\sigma}_o = 0.25$, (b) $\Delta p/\bar{\sigma}_o = 0.5$, and (c) $\Delta p/\bar{\sigma}_o = 0.75$, in the *model with residual friction* (Figure 1b) $f_r/f_p = 0.6$. Dotted lines correspond to the model with unlimited friction weakening (Figure 2). The two models are equivalent for $\delta_{|x\,=\,0} \le \delta_r \equiv (1 - f_r/f_p)\delta_w$. Lighter lines correspond to the small scale yielding (s.s.y.) asymptote. The case of $\tau^b/\tau_p = 0.55$ in Figure 9b shows quasi-static evolution of the crack toward the point of instability A, followed by dynamic propagation episode (vertical arrow), which is arrested at point B, after which the crack resumes quasi-static expansion.

propagation is the necessary condition for the arrest, while the sufficiency has not been established here, and may require explicit solution for dynamic crack propagation. To this end, *Viesca and Rice* [2012] used numerical simulations of dynamic rupture nucleated on a fault with limited slip-weakening in a similar problem. They show that the dynamic rupture is indeed arrested at/near the states predicted from the quasi-static solution with a limited amount of dynamic overshoot.

5.2. Small Scale Yielding

[45] Fault responses to the pressurization observed in the model with a residual fault friction fall in two general categories of ultimately *stable* (with or without a dynamic episode) and ultimately *unstable* slips. The corresponding criteria, as well as the relevant asymptotic behavior of the fault can be discerned from the analysis when the quasi-static crack length is large compared to the characteristic value a_w, such that the strength slip-weakening is localized to a small zone near the crack tip. In fact, this localization can be directly observed from the slip and stress distributions corresponding to the solutions shown in Figures S2b and S2c in the auxiliary material. In this case, we use the small scale yielding (s.s.y.) approach [*Rice*, 1968; *Palmer and Rice*, 1973] and evaluate the fracture energy as

$$G^* \simeq \left(f_p - f_r\right)\overline{\sigma}(a)\frac{\delta_r}{2} \tag{27}$$

on the assumption that the effective normal stress is approximately constant within the (small) end zone and equal to $\overline{\sigma}(a)$.

[46] On the other hand, the stress intensity factor (SIF), K, that would exist at a tip of the crack, loaded by the far field stress τ^b and by the shear traction equal to the *residual* fault strength $f_r\overline{\sigma}$, can be written as a sum of the SIF at ambient conditions and the perturbation ΔK due to the pressurization:

$$K = \left(\tau^b - \tau_r\right)\sqrt{\pi a} + \Delta K(a,t), \tag{28}$$

where

$$\Delta K(a,t) = f_r\sqrt{\frac{a}{\pi}}\int_{-a}^{a}\frac{p(x,t)-p_o}{\sqrt{a^2-x^2}}dx \tag{29}$$

and $\tau_r = f_r\overline{\sigma}_o$ is the residual strength at ambient conditions. This allows for the evaluation of the rate $G = K^2/(2\mu^*)$ at which the elastic energy can be quasi-statically released into a crack tip region in the event of crack propagation. Then, the crack propagation criterion $G = G^*$, or, equivalently,

$$K^2/(2\mu^*) = G^*, \tag{30}$$

yields the asymptotic solution for the crack length a.

[47] This asymptotic solution is generally in good agreement with the full numerical solution when the crack is large enough. We do not show it here, because a more accurate version of the s.s.y. solution can be obtained by replacing a in (28) with an effective crack length $a_{\text{eff}} = a - 0.466d$ (Appendix D), where $d = 0.466(\pi/2)(\overline{\sigma}_o/\overline{\sigma}(a))a_w$ is the size of the end zone [*Dempsey et al.*, 2010]. This improved s.s.y. solution, plotted by gray lines in Figure 9 (left), is in excellent agreement with the full solution when $a \gtrsim 2a_w$.

5.3. Ultimate Stability

[48] The condition for the ultimate stability of the pressurized fault requires that the slipping patch can be stably (quasi-statically) grown to the infinite size in infinite pressurization time, or, in other words, that the s.s.y. solution possesses the asymptotic limit of $a \to \infty$ when $t \to \infty$. Rewriting (29) as $\Delta K(a,t) = f_r\sqrt{\frac{a}{\pi}}\int_{-1}^{1}\frac{p(as,t)-p_o}{\sqrt{1-s^2}}ds$ and taking into account that in our case (i.e., fluid diffusion) $p(as, t) - p_o > 0$ and momothonically decreases with increasing a, we observe that the integral in ΔK decreases with a. This suggests that ΔK either decreases with a or, at least, grows slower than $\sqrt{a}$ as $a \to \infty$. Therefore, the first term in (28) is the leading one and $K \to -\infty$ if

$$\tau^b < \tau_r \tag{31}$$

In reality, negative values of K are unattainable because the patch will stop growing as soon as K becomes less than $\sqrt{2\mu^* G^*}$. Its further growth is only possible when the pressure increases to maintain $K = \sqrt{2\mu^* G^*}$. Hence the necessary and sufficient condition (31) implies that stable, quasi-static growth of the slipping patch during sustained fault pressurization requires that the background stress value is less than the value of the residual fault strength at ambient conditions.

[49] When $\tau^b > \tau_r$, $K \to \infty$ as $a \to \infty$ in (28). We, therefore, predict, not surprisingly, an imminent fault slip instability if $\tau^b > \tau_r$.

[50] Note that the stability criterion (31) is in agreement with the numerical solution for the development of the quasi-static slipping patch on a fault with residual friction $f_r/f_p = 0.6$ (Figure 9). In this case, the neutrally stable trajectory corresponds to $\tau^b/\tau_p = \tau_r/\tau_p = 0.6$ while the solution trajectories for higher and lower background stresses correspond to ultimately dynamic and quasi-static slip, respectively (Figures 9b and 9c). The above asymptotic consideration suggests that for $\tau^b/\tau_p < \tau_r/\tau_p = 0.6$, crack length a increases quasi-statically at large times. Hence, the crack growth is stable at $t \to \infty$, which would be difficult to establish purely numerically. We also note that a large enough pressure perturbation, $\Delta p/\overline{\sigma}_o \geq 1 - f_r/f_p$, is required in order to activate slip, (6), on an ultimately stable fault, (31).

5.4. Large Nucleation Patch Near Stable-to-Unstable Transition ($\tau^b \simeq \tau_r$)

[51] When τ^b is just above the residual strength τ_r, the length of the final nucleation patch is large and its front is well ahead of the "front" of the pressurized zone (also large). This means that $a \gg \sqrt{\alpha t} \gg a_w$ and $\overline{\sigma}(a) \simeq \overline{\sigma}_o$, which can be seen, for example, for the $\tau^b/\tau_p = 0.65$ trajectory in the left parts of Figures 9b and 9c. We note that the separation of scales between the slipping patch and the pressurized zone also arises on critically stressed faults ($\tau^b \simeq \tau_p$, Figure 4b), but in this case, the nucleation patch scales with a_w while the pressurized zone is small (i.e., $a \sim a_w \gg \sqrt{\alpha t}$).

[52] A "point force" asymptote, $p(x,t) - p_o \simeq \Delta P(t)\delta_{Dirac}(x)$, can be used again to represent a relatively small pressurized region, centrally located within the crack, when evaluating the corresponding contribution to the stress intensity factor. Then $\Delta K(a, t) = f_r\Delta P(t)/\sqrt{\pi a}$ in (28). Differentiating propagation criterion (30) in time, and passing to the nucleation

limits, $a \to a_c$ and $da/dt \to \infty$, we find that $\Delta K = \Delta K_c = (\tau^b - \tau_r)\sqrt{\pi a_c}$ at the nucleation. Substituting this expression back in (30), we recover the large nucleation patch asymptote,

$$\frac{a_c}{a_w} \simeq \frac{1}{4\pi}\left(\frac{\tau_p - \tau_r}{\tau^b - \tau_r}\right)^2 \qquad (\tau^b \to \tau_r + 0). \tag{32}$$

The corresponding nucleation time is recovered from $\Delta K(a_c, t_c) = \Delta K_c$. As above, a more accurate asymptote is obtained from (32) by replacing a_c with the effective nucleation size of $a_c - 0.341a_w$ (Appendix D).

[53] Equation (32) was independently reported by *Viesca* [2011]. Expressing the characteristic length (11) in terms of the slip-weakening distance δ_r and substituting the result, $a_w = \mu^*\delta_r/(\tau_p - \tau_r)$, in (32), one obtains the expression which agrees (up to a factor of 1/4) with *Andrews*' [1976] critical crack length L_c. The similarity between the large a_c asymptote (32) and L_c reflects the s.s.y. nature of the corresponding shear crack solutions. The difference in the prefactor reflects different loading conditions. That is, a_c in (32) appears from the point-force-like pore pressure distribution applied at the center of the crack (combined with the background stress), while L_c in *Andrews*' [1976] work is the minimum length for a propagating crack loaded only by the uniform background stress.

5.5. Large Dynamic Run-Out on a Marginally Pressurized ($f_p\Delta p \simeq \tau_p - \tau^b$), Aseismic ($\tau^b < \tau_r$) Fault

[54] In seismology, "aseismic" faults are often defined as creeping faults that never host a dynamic rupture. This definition is typically constrained by excluding earthquakes of sufficiently small magnitude (e.g., micro earthquakes) or not consistent with the fault plane. In the history of fault evolution, however, the loading conditions or fault strength may change resulting in sizable seismic events and dynamic rupture on the fault that previously was aseismic [e.g., *McGuire et al.*, 1997]. In this work, a fault is considered to be aseismic in its current state, that is, before the onset of change of the background loading, fluid pressure, or rock strength. To avoid confusion, we define a fault to be aseismic if prestress τ^b is less than the residual fault strength τ_r at the ambient conditions.

[55] In the case of marginally pressurized aseismic faults, the nucleation time is large and the corresponding size of the pressurized region is much larger than the nucleation patch size (Figure 4a), resulting in the large run-out distances of the dynamic rupture before the arrest, so that $a = a_{\text{arrest}} \gg a_w$. Indication of this behavior can be seen in Figure 9b (left) for values of the background stress τ^b/τ_p approaching the minimum value $1 - \Delta p/\overline{\sigma}_o = 0.5$ required to activate the quasi-static slip for the considered value 0.5 of the overpressure $\Delta p/\overline{\sigma}_o$ (further discussed in section 5.6). Since $K = \sqrt{2\mu^* G^*}$ in (30) is bounded, (28) suggests that to the first-order $\Delta K \simeq (\tau_r - \tau^b)\sqrt{\pi a}$ when $a \gg a_w$. The corresponding asymptotic expressions for the arrested crack length and dynamically accrued peak slip (at the crack center when it is arrested) on a marginally pressurized fault are given in Appendix E.

[56] These asymptotes suggest that for a given value of the residual friction, the run-out distance roughly tracks the pressurized fault length $\sim\sqrt{\alpha t_c}$ (see, e.g., (17) and (19) for particular pressurization scenarios) and the peak accrued slip $\sim(\tau_p/\mu^*)\sqrt{\alpha t_c}$. The exception to these estimates corresponds to the vicinity of the lower (upper) bound of the understress and overpressure when the run-out distance is much larger (smaller) than the size of the pressurized region. The lower and upper bounds of the understress and overpressure on a marginally pressurized fault correspond to the transition to the ultimately unstable fault behavior ($\tau^b = \tau_r$) and to hydraulic fracturing ($\Delta p = \overline{\sigma}_o$), respectively.

5.6. Main Results for the Effects of Residual Friction

[57] The main findings of the numerical solutions and asymptotic analyses are illustrated in Figures 10 and 11 in the case (8) of constant overpressure. Figure 10 shows the crack length (left) and peak slip (right) at the (re-) nucleation and arrest of dynamic rupture on a fault with $f_r/f_p = 0.6$ as a function of the fault understress for the same three values of the fluid overpressure considered previously in Figure 9. Figure 11 maps all stable and unstable regimes of slip evolution (as discussed in this section and illustrated in numerical examples in Figures 9 and 10) in the parametric space of the understress and overpressure. A similar regime map in the case (9) of injection with constant flow rate is shown in Figure S5 in the auxiliary material.

[58] According to the asymptotic analysis (sections 5.2 and 5.3), a fault is ultimately unstable when the background stress magnitude exceeds the residual static strength at the ambient pore pressure (i.e., when $\tau^b > \tau_r$). This agrees with the numerical results (Figure 10) for $\tau_p - \tau^b < \tau_p - \tau_r = 0.4\tau_p$ or $\tau^b > \tau_r = 0.6\tau_p$. The nucleation of unstable sliding takes place on "smaller" patches within the range defined by (24) and (25) when τ^b is sufficiently larger than τ_r, and the fault residual strength is not reached in the course of the slip leading to the nucleation (i.e., $\tau > \tau_r$, see region 2a in Figure 11). The (re-) nucleation of dynamic slip on "larger" patches (32) takes place when τ^b approaches τ_r from above (regions 2b and 3 in Figure 11) and a large part of the slipping patch has achieved the residual friction. This can be seen, for example, for ranges (0.26, 0.4) and (0.2, 0.4) of the normalized understress $(\tau_p - \tau^b)/\tau_p$ in Figures 10b and 10c, respectively.

Figure 10. (left) Crack half-length and (right) slip at the crack center at the nucleation, arrest, and re-nucleation of dynamic rupture as functions of understress $(\tau_p - \tau^b)/\tau_p$ for fixed values of the overpressure $\Delta p/\overline{\sigma}_o = \{0.25, 0.5, 0.75\}$ in the *model with residual friction* $f_r/f_p = 0.6$ and constant pressure source (8). Dashed lines show the normalized position of the pressure diffusion "front," $\sqrt{\alpha t_c}/a_w$, at the (re-) nucleation. The rate of dynamic slip per unit crack advance (from the nucleation to arrest) is shown in Figures 10b and 10c, right axis. For larger values of the overpressure (Figures 10c and 10d) the nucleation length/peak slip in the model with residual friction differs from that in the model with unlimited weakening (dotted line in Figure 10c) in a range of the background stress τ^b. In the case with residual friction, nucleation is suppressed all together on ultimately stable faults ($\tau^b < \tau_r$), with the exception for a small range of low τ^b values near the marginal-pressurization condition (Figure 10c). This range vanishes as $\Delta p \to \overline{\sigma}_0$ (Figure 10d).

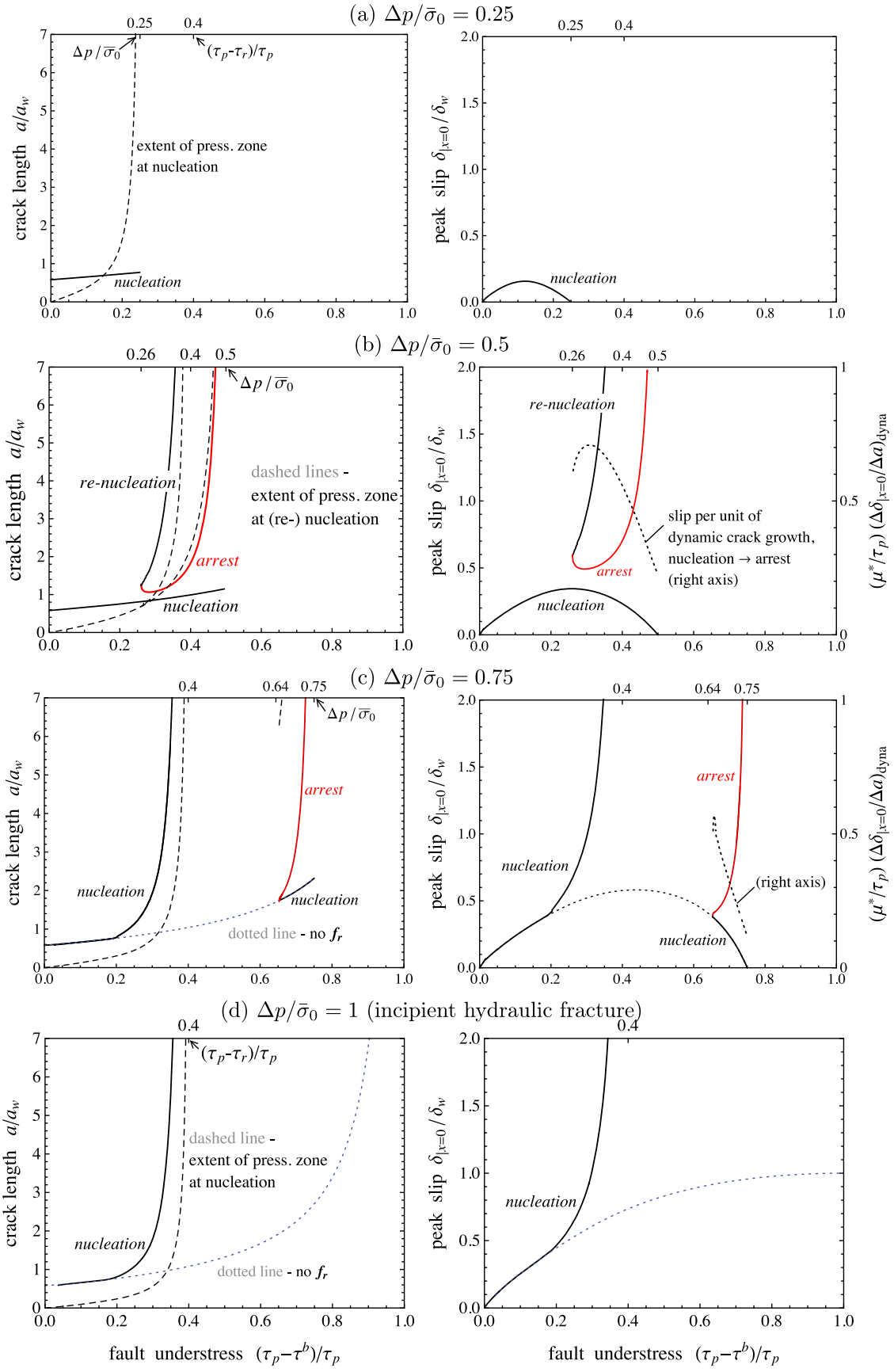
(a) $\Delta p/\bar{\sigma}_0 = 0.25$
0.25
0.4
$\Delta p/\bar{\sigma}_0$
$(\tau_p-\tau_r)/\tau_p$
extent of press. zone
at nucleation
nucleation
crack length a/a_w
peak slip $\delta_{|x=0}/\delta_w$
(b) $\Delta p/\bar{\sigma}_0 = 0.5$
0.26
0.4
0.5
re-nucleation
arrest
dashed lines -
extent of press. zone
at (re-) nucleation
slip per unit of
dynamic crack growth,
nucleation → arrest
(right axis)
$(\mu^*/\tau_p)\,(\Delta\delta_{|x=0}/\Delta a)_{\rm dyna}$
(c) $\Delta p/\bar{\sigma}_0 = 0.75$
0.64
0.75
dotted line - no f_r
(right axis)
(d) $\Delta p/\bar{\sigma}_0 = 1$ (incipient hydraulic fracture)
dashed line -
extent of press. zone
at nucleation
fault understress $(\tau_p-\tau^b)/\tau_p$

Figure 10

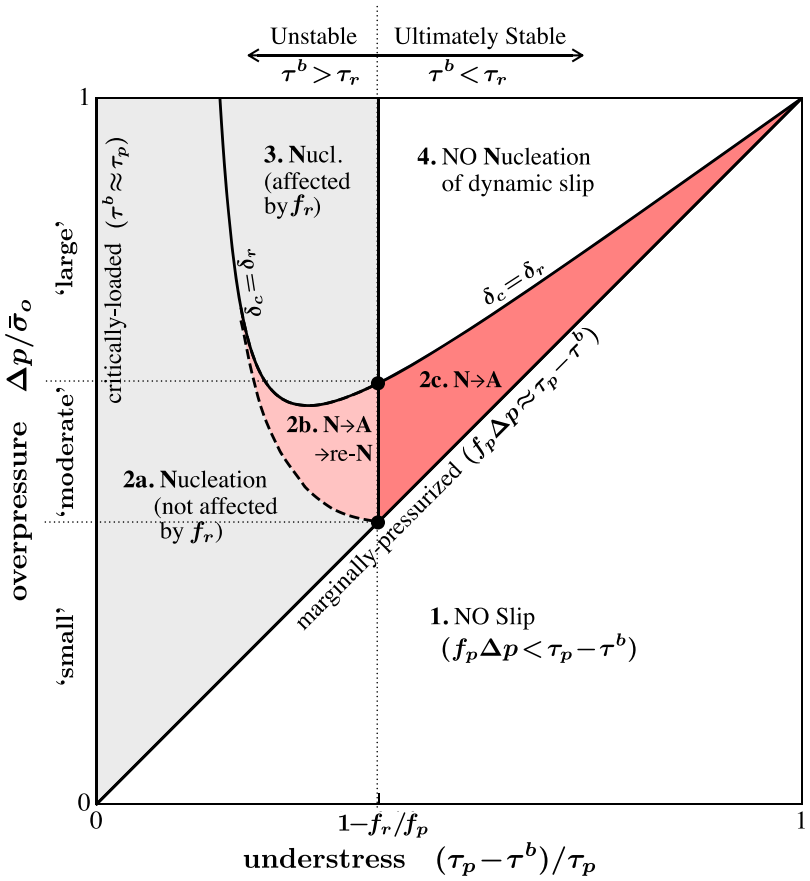

Figure 11. Map of different slip regimes in the space of the normalized understress $(\tau_p - \tau^b)/\tau_p$ and overpressure $\Delta p/\bar{\sigma}_o$ for $f_r/f_p = 0.6$. 1. No fault slip (overpressure is not sufficient to activate slip). 2. Nucleation of dynamic slip is not affected by the residual friction f_r (i.e., the slip at nucleation δ_c is less than δ_r); distinct sub-regimes correspond to different outcomes of dynamic slip, that is, (2a) unabated dynamic rupture, (2b) arrest, followed by re-nucleation of unabated dynamic rupture, and (2c) arrest (ultimately stable fault). 3. Nucleation of dynamic slip, affected by f_r, leading to unabated dynamic rupture. 4. No dynamic slip nucleation for "large" overpressure on ultimately stable fault. Dependencies of the crack length and the peak slip at the nucleation, arrest, and re-nucleation on the understress for different values of overpressure (from the 'small', 'moderate', and 'large' overpressure ranges, as defined in the Figure) are illustrated in Figures 10a, 10b, 10c, and 10d, respectively. The line $\delta_c = \delta_r$, which separates the parametric regions where dynamic instability is and is not affected by the level of the residual friction f_r, respectively, is evaluated from the solution with unlimited friction slip-weakening (Figure 8e).

[59] Faults are ultimately stable when $\tau^b < \tau_r$, but the pattern of slip development depends on the level of pressurization and that of the background stress. For sufficiently large fluid overpressure (e.g., for $\Delta p/\bar{\sigma}_o = 0.75$ in Figure 10c), no nucleation of dynamic rupture takes place when the residual fault strength is reached within the quasi-statically expanding slipping patch (regime 4, Figure 11). Such behavior is characteristic for intermediate values of the fault loading, which maximize quasi-static slip ($0.4 < (\tau_p - \tau^b)/\tau_p < 0.64$ in Figures 10c). This stabilizing trend with increasing overpressure persists as the overpressure is increased to the level of the ambient effective stress ($\Delta p/\bar{\sigma}_o = 1$ in Figure 10d), which corresponds to the incipient hydraulic fracturing condition at the fluid source. In this case, dynamic rupture is suppressed entirely in the ultimately stable fault loading range, $\tau^b < \tau_r$, (corresponding to the understress range $0.4 < (\tau_p - \tau^b)/\tau_p < 1$ in Figures 10d and 11).

[60] On the other hand, for moderate to large overpressure ($\Delta p/\bar{\sigma}_o > (\tau_p - \tau_r)/\tau_p$ in Figures 10b, 10c, and 11), nucleation of dynamic rupture on "small" patches is followed by the eventual arrest when the background stress is sufficiently low (regime 2c in Figure 11).

[61] Finally, we note that longer run-out distances of the dynamic rupture and larger dynamically accumulated slip are expected for marginally pressurized faults, when the fluid overpressure is at the minimum required to activate the fault slip (i.e., $(\tau_p - \tau^b)/\tau_p \to \Delta p/\bar{\sigma}_o$ in Figures 10b and 10c). Large run-out distances may favor activation of other (dynamic) fault weakening mechanisms during a prolonged dynamic slip episode that, in turn, may lead to a run-away dynamic rupture

and a larger earthquake. This effect of dynamic weakening mechanisms is discussed below.

6. Effect of Dynamic Weakening

[62] Can dynamic rupture, that is otherwise bound for arrest under conditions (26) of limited quasi-static weakening, run-away? Our model with the residual quasi-static friction predicts that faults with background loading less than the residual strength (equation (31)) are ultimately stable, yet may exhibit an episode of dynamic slip (e.g., region 2c in Figure 11) confined to the zone with perturbed pore pressure. Interestingly, dynamic ruptures nucleated on marginally pressurized faults tend to run out the longest distance prior to the arrest (e.g., Figure 10, left), owing to the fact that nucleation under the marginal pressure conditions requires a pressurized region far-exceeding the length of the fracture at the initial instability. It is plausible to think that the longer the distances of dynamic crack propagation and, therefore, the higher the dynamically accumulated slip on the fault (Figure 10, right), the higher the likelihood that other (dynamic) weakening mechanisms can be activated in the course of a dynamic rupture episode. These mechanisms may allow rupture to propagate dynamically beyond the otherwise predicted arrested length. This would constitute a scenario of an earthquake nucleation on a statically strong, but dynamically weak fault [*Lapusta and Rice*, 2003; *Rice*, 2006; *Noda et al.*, 2009]. This possibility is examined below for two generic dynamic weakening mechanisms related to the frictional heating in the course of seismic slip.

6.1. Flash Heating on Asperities

[63] The first mechanism corresponds to the "flash heating on microscopic asperities" along a thin principal shear zone [*Rice*, 2006, and references therein], resulting in significant reduction of the macroscopic friction in laboratory experiments when the slip rate exceeds a threshold value of ~0.1 m/s [e.g., *Di Toro et al.*, 2011]. A dynamic rupture episode in the model with residual quasi-static friction (for sufficiently low values of the background stress) is characterized by the average normalized rate of slip, $(\Delta\delta/\Delta a)_{dyna} \sim \tau_p/\mu^*$, per unit of dynamic crack growth increment (Figures 10b and 10c, heavy-dotted lines, right axes). The corresponding average dynamic slip rate is estimated by

$$V_{\mathrm{dyna}} \sim v_r(\Delta\delta/\Delta a)_{\mathrm{dyna}} \sim v_r\tau_p/\mu^*,$$

where v_r is the velocity of dynamic rupture propagation. Assuming $v_r \sim 1$ km/s, $\tau_p \sim 20$–100 MPa (which roughly corresponds to 1–7 km depth), and $\mu^* \sim 30$ GPa, we estimate $V_{\mathrm{dyna}} \sim 0.6$–$3$ m/s > 0.1 m/s. This simple consideration shows that the flash heating mechanism can be realistically activated during a dynamic rupture episode following the initial fault instability. Therefore, this mechanism can potentially prevent the arrest, predicted otherwise, leading to the unabated dynamic propagation (and a large earthquake). We note, however, that an explicit solution for the dynamic rupture propagation driven by the slip-rate weakening ("flash heating") mechanism is necessary to validate the latter possibility, which is outside the scope of this paper.

6.2. Thermal Pressurization

[64] Another generic mechanism of dynamic fault weakening corresponds to thermal pressurization resulting from the mismatch between the thermal expansivity of the pore fluid and that of the pore space [*Sibson*, 1973; *Lachenbruch*, 1980]. This mismatch leads to the fluid pressure increase with accumulated slip, unless diffusion and/or fault gouge dilatancy [e.g., *Garagash and Rudnicki*, 2003] is efficient enough to dissipate such increases. During the quasi-static fault slip, the timescale of the pore pressure diffusion across the thickness of the principal shear zone is likely to be much smaller than the timescale of the frictional heating, which effectively suppresses thermal pressurization (e.g., for seismogenic crust) [*Segall and Rice*, 2006]. On the contrary, during the dynamic slip, the rate of diffusion may be well below the rate of shear heating, resulting in essentially undrained, adiabatic response of the principal shear zone and in the maximum thermal pressurization effect. We further assume that the latter is true during a dynamic rupture episode, resulting in the following undrained, adiabatic pressurization equations along the fault [*Lachenbruch*, 1980]:

$$dp - \Lambda dT = 0, \qquad \rho ch\, dT = \tau d\delta. \tag{33}$$

These equations represent the fluid balance under the undrained conditions, and the energy balance for the principal shear zone of thickness h under the adiabatic conditions, respectively. Here T is the temperature, Λ is the undrained pressurization coefficient, and ρc is the volumetric heat capacity of the fault gouge. In view of the explicit dependence (4) of the fault frictional strength on slip, equations (33) can be integrated to obtain the slip-dependence of the pressure, and, consequently, of the fault strength, as follows:

$$\tau = f(\delta)\bar{\sigma}_i \exp\left(-\frac{\Lambda}{\rho ch}\int_{\delta_i}^{\delta} f(\delta)d\delta\right), \tag{34}$$

where δ_i and $\bar{\sigma}_i = \sigma_n - p_i$ are certain initial values of the slip and the effective normal stress, respectively. In the context of the dynamic slip nucleation and ensuing activation of the thermal pressurization mechanism, the initial state in (34) corresponds to that at the instability of the quasi-static slip, i.e., $\delta_i(x) = \delta(x, t_c)$ and $\bar{\sigma}_i(x) = \sigma_n - p(x, t_c)$. The extent of dynamic slip weakening, associated with the exponential term in (34), depends on the cumulative dynamic slip, $\delta - \delta_i$, in relation to the characteristic slip-weakening distance, that can be defined as $(\delta_w)_{dyna} = \rho ch/(f_p\Lambda)$. Since the maximum dynamic slip is $\sim\delta_w$ for arrested dynamic ruptures in the model without the dynamic weakening (Figures 10b (right) and 10c (right), the dynamic fault weakening in that range of slip is scaled by the ratio $\delta_w/(\delta_w)_{dyna}$ (except for conditions of marginally pressurized fault where the dynamic slip may be much larger, and so would be the anticipated dynamic weakening). For crustal rocks, $\rho c \sim 3$ MPa/°C, $\Lambda \sim 1$ MPa/°C, $f_p \sim 0.6$ [e.g., *Lachenbruch*, 1980; *Rice*, 2006], so $(\delta_w)_{dyna} \sim 5h$. The principal shear zone thickness h is not well constrained. Sub-mm to cm values of h have been suggested for seismic slip on mature faults [*Wibberley*, 2002; *Chester et al.*, 2004; *Rice*, 2006]. Such small values may have resulted from multiple, severe localization events of slip [*Platt et al.*, 2010], but larger values cannot be ruled-out at the earthquake nucleation or for shear fractures propagating through fresh rock. Thus,

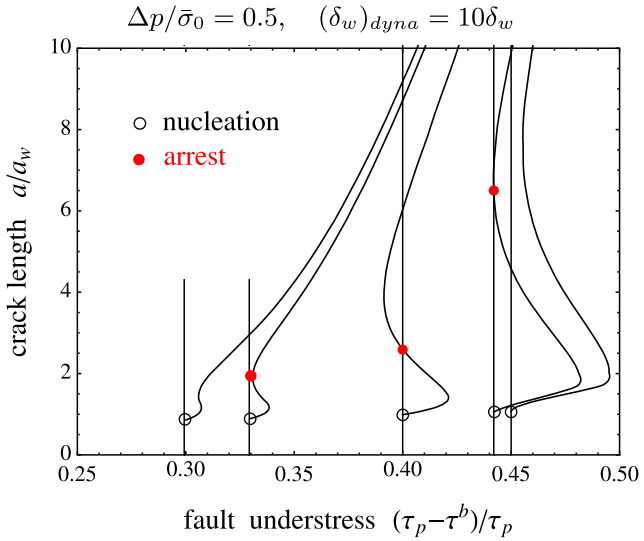

Figure 12. Example of "quasi-static" calculations to determine the effect of a dynamic slip-weakening mechanism (thermal pressurization of the shear zone under undrained, adiabatic conditions) on the arrest of dynamic rupture in the model with residual friction $f_r/f_p = 0.6$ and fixed fluid overpressure $\Delta p/\bar{\sigma}_o = 0.5$. For a given value of the background stress τ^b, the thermal pressurization mechanism is switched on and the injection is stopped at the instability ($t = t_c$ and $a = a_c$) of the quasi-static crack growth (shown with an open circle). Past this moment, a fictitious quasi-static growth solution, which now includes τ^b as an unknown, is evaluated for incremented crack length $a > a_c$. During the latter stage, the undrained shear strength decays over slip distances $\sim(\delta_w)_{dyna} = (\rho c/f_c\Lambda)h$, where ρc is the gouge heat capacity, f_c is the friction coefficient at the instability, $\Lambda = dp/dT$ is the undrained thermal pressurization factor, and h is the thickness of the principal shear zone. The arrest conditions are met at $a_{\text{arrest}} > a_c$ (shown by a red dot) if the value of τ^b in the fictitious quasi-static solution reaches the true value of τ^b there (indicated by a vertical line). The solution shows that the arrest condition is met over a narrower range of background stress, $0.33 \lesssim \tau^b/\tau_p \lesssim 0.44$, than in the solution without the dynamic weakening, $0.26 \lesssim \tau^b/\tau_p \lesssim 0.5$ (Figure 10b).

$(\delta_w)_{dyna}$ may be roughly in mm to decimeter range, which, in view of a plausible sub-mm to mm range for δ_w (see further in section 7.2), suggests that the magnitude of the dynamic fault weakening due to thermal pressurization (scaled by the ratio $\delta_w/(\delta_w)_{dyna}$) is small for all but the marginally pressurized initial fault conditions.

[65] Dependence (34) of the undrained-adiabatic thermal pressurization on the slip (but not on the slip rate) allows us to develop conditions for possible arrest of dynamic rupture without referring to explicit dynamic solutions. Indeed, the arrested state of the dynamic rupture can be described by a quasi-static crack solution for the same strength-slip relation (34). Thus, the necessary arrest condition corresponds to the existence of such a quasi-static solution with $a > a_c$ and slip exceeding $\delta(x, t_c)$.

[66] To simplify the task of numerical search for the arrested slip solutions, we solve for fictitious quasi-static growth of the crack past the instability ($a > a_c$) when the fault strength is described by (34) by incrementing the crack length $a > a_c$ while allowing the background stress τ^b to change from its true value. The state of the arrested dynamic growth is recovered when the value of τ^b in the fictitious solution returns to its true value (if it does).

[67] The piecewise constant slip numerical method outlined in section A2 is used for the fictitious quasi-static crack solution. Examples of these solutions and the corresponding arrested states (when they exist) are shown in Figure 12 for several values of the true background stress (or the understress), as indicated by the intercepts of the vertical lines, and the fixed value of the fluid overpressure $\Delta p/\bar{\sigma}_0 = 0.5$ in the model with residual friction $f_r/f_p = 0.6$ and $\delta_w/(\delta_w)_{dyna} = 0.1$. The two arrested states with the vertical tangent at the corresponding true values of the fault understress define the range for the rupture arrest. This range is reduced compared to the one without the dynamic weakening mechanism, as further examined in Figure 13 for various values of the characteristic slip weakening distance ratio $\delta_w/(\delta_w)_{dyna}$. The arrest range of the understress is reduced from $0.26 \le (\tau_p - \tau^b)/\tau_p \le 0.5$ for the zero value of the ratio (no dynamic weakening) to an empty set for $\delta_w/(\delta_w)_{dyna} \gtrsim 0.14$.

[68] The magnitude of the dynamic weakening due to the thermal pressurization of pore fluid is estimated to be relatively small due to the fact that most of dynamic weakening is expected to occur at the slip scale of $(\delta_w)_{dyna}$, which is likely larger than the slip $\sim\delta_w$ that would be accumulated during a dynamic rupture episode without dynamic weakening effects. Yet we observe from the above example that the effect of the dynamic weakening to increase the rupture run-out distance is not negligible for $\delta_w/(\delta_w)_{dyna} \gtrsim 0.1$.

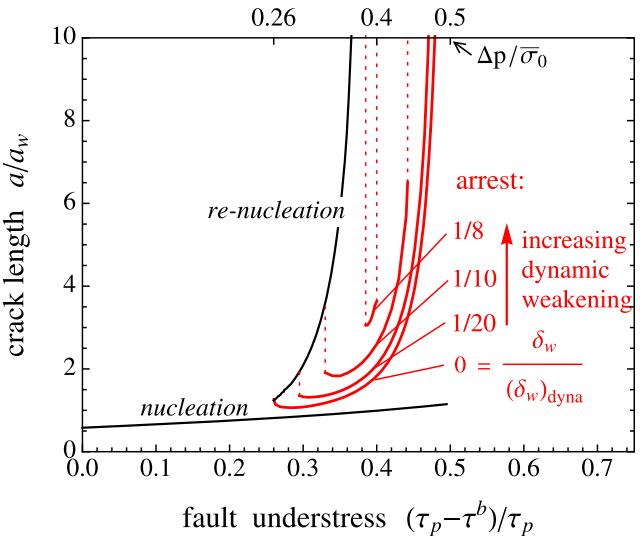

Figure 13. Crack half-length at the arrest of dynamic propagation as a function of the background stress for various degrees of dynamic weakening, $\delta_w/(\delta_w)_{\text{dyna}} = \{0, 0.05, 0.1, 0.125\}$, in the model with residual friction $f_r/f_p = 0.6$ and fixed overpressure $\Delta p/\bar{\sigma}_o = 0.5$. Increasing the ratio of the static-to-dynamic slip weakening distances corresponds to increasing dynamic weakening, with the zero value equivalent to no dynamic weakening (Figure 10b). The range of background stress where the arrest condition is met shrinks with increasing effect of the dynamic weakening and vanishes for $\delta_w/(\delta_w)_{\text{dyna}} \gtrsim 0.14$.

Furthermore, values of this ratio as low as 0.14 (for the considered value of the overpressure $\Delta p/\overline{\sigma}_0 = 0.5$) eliminate the possibility for the rupture arrest and lead to the unabated seismic slip in the entire range of the fault uniform prestress. At least, in the confines of our simplified fault model.

7. Discussion

7.1. Assumption of Rate-Independent Slip Weakening

[69] The classic concept of the rate- and state- dependent friction [*Dieterich*, 1979; *Ruina*, 1983] can be described, for example, by the friction "ageing" law [*Ruina*, 1983]

$$\tau = \bar{\sigma}\left[f_o + a\ln\frac{V}{V_o} + b\ln\frac{\theta}{\theta_o}\right], \qquad \frac{d\theta}{dt} = 1 - \frac{V\theta}{d_c}, \qquad (35)$$

where θ is the state variable, d_c is the characteristic strength-evolution slip distance, a (not to be mistaken for the crack half length a or a_c used otherwise in this work) and b are the frictional parameters quantifying the dependence of friction on slip rate and "state" of the frictional surface, respectively, and f_o is the frictional coefficient at the reference rate V_o and state θ_o. Considering large slip rates such that $V\theta/d_c \gg 1$, *Uenishi and Rice* [2003] suggested that (35) can be approximated by a linear slip-weakening law for small values of ratio a/b. This has been confirmed by *Rubin and Ampuero* [2005], who recovered the *Uenishi and Rice* [2003] nucleation length scale [see also *Dieterich*, 1992]

$$a_c \sim \frac{\mu^*}{w\overline{\sigma}_0} \qquad (36)$$

for the nucleation patch when $a/b \ll 1$. Here $w = b/d_c$ is the slip-weakening rate of friction when recast in terms of rate and state friction parameters, b and d_c. *Rubin and Ampuero* [2005] and *Ampuero and Rubin* [2008] have further shown that the nucleation patch length scale increases with increasing ratio a/b from the minimum value given by (36) to the following asymptotic form as $a/b \to 1$:

$$a_c = \frac{1}{\pi}\left(\frac{\tau_p - \tau_r}{\tau^b - \tau_r}\right)^2 \frac{\mu^*}{w\overline{\sigma}_0} \qquad (37)$$

Here $\tau_p - \tau_r \propto b\overline{\sigma}_0$ is the frictional strength drop from the peak (τ_p) to the residual (τ_r) strength level, which is accomplished in the small end-zones near the tips of the nucleation patch, and $\tau^b - \tau_r \propto (b - a)\overline{\sigma}_0$ is the stress drop from the background (τ^b) to the quasi-uniform residual ($\approx\tau_r$) level in the interior of the patch. Substituting the expression for the slip-weakening stress rate in terms of the strength drop over the slip-weakening distance δ_r, $w\overline{\sigma}_0 = (\tau_p - \tau_r)/\delta_r$ in (37), shows that this nucleation length scale is identical to the *Andrews*' [1976] expression for the maximum extent of a slip-weakening, quasi-static crack, before the onset of dynamic propagation. *Uenishi and Rice*'s [2003] study has not yielded the nucleation length scale (37) due to the unlimited nature of friction weakening in their model. As shown in section 5.4, nucleation in a slip-weakening model with residual friction does recover length scale (32), which is similar to (37), when the prestress value is close to the residual value of the ambient strength. In other words, length scale (37) can be interpreted in the framework of a slip-weakening model with residual friction when most of the weakening takes place near the fracture tips (small scale yielding).

[70] "Rate and state" frictional law (35) with fixed d_c is experimentally justified for some fault conditions, such as low velocity (aseismic) sliding on bare rock surfaces or on thin gouge layers [e.g., *Marone*, 1998]. This law, however, does not necessarily work well for sliding on thicker gouge layers where redistribution and localization of shear strain with incurred slip [e.g., *Marone et al.*, 1992; *Beeler et al.*, 1996] is likely to correspond to changing the state evolution distance d_c with evolving shear zone thickness and may lead to a change of frictional stability (sign of $a - b$). The evidence of non-trivial internal structure and slip localization within ultra-cataclastic gouges of exhumed mature fault zones [e.g., *Chester et al.*, 1993; *Chester and Chester*, 1998; *Wibberley and Shimamoto*, 2003] is well established. Although the slip-weakening friction law is not always physically justified, it does adequately describe the post-failure phase of triaxial compression of granite [*Rummel et al.*, 1978; *Rice*, 1980; *Wong*, 1986], and the post-localization stage in plane-strain compression of cohesionless materials (a proxy for fault gouge) [e.g., *Han and Vardoulakis*, 1991]. Furthermore, if the rate- and state- dependent framework is a valid physical representation of the fault friction (e.g., for aseismic slip on bare rock surfaces [*Marone*, 1998]), the above correspondence of the end-members indicate that the simplified slip-weakening friction framework may be asymptotically accurate at least in the limits of $a/b \ll 1$ and $a/b = 1$.

7.2. Slip Weakening Scale, Nucleation Length, and Dynamic Run-Out Distance

[71] *Uenishi and Rice* [2003] suggest that a laboratory-derived rate- and state-dependent ageing friction law (35) for an established slip surface [*Ruina*, 1983] can be approximated, over a range of slip distances, by a linear slip dependence (5) with the slip-weakening rate $w \approx b/d_c$, where $b \approx 0.015$ and $d_c \approx 5$ to 100 μm are the typical values of the friction parameter and the state-evolution distance [e.g., *Marone*, 1998], respectively. They further find that the calculated range of $w \approx 0.15$ to 3/mm is broadly consistent with the values of slip-weakening rate $W = w\overline{\sigma}_0$ of the frictional strength inferred by *Rice* [1980] and *Wong* [1986] from the post-failure stage of triaxial experiments on initially intact granite specimens [*Rummel et al.*, 1978]. For characteristic values $w \approx 0.7$/mm, $f_p = 0.8$, $\mu^* \sim 30$ GPa, and $\overline{\sigma}_o \sim 50$ MPa (ambient conditions at 3 km depth), the characteristic slip and the characteristic crack length are $\delta_w = f_p/w \approx 1.2$ mm and $a_w = (\mu^*/\tau_p)\delta_w \approx 0.9$ m, respectively. Roughly an order of magnitude variation centered about these values is plausible according to the estimated range for w.

[72] As seen from equations (24) and (25) and Figures 8a and 8b, the crack length at the nucleation of dynamic rupture scales with a_w through the strength-stress ratio: $2a_c \approx 1.2(\tau_p/\tau^b)a_w$. Thus, the nucleation patch is at its minimum size $\approx$1.1 m on critically stressed (favorably oriented) faults, and increases inversely proportionally to the decreasing background stress for less critically loaded faults. The minimum possible size of an induced seismic event in the crust corresponds to the dynamic slip on a favorably oriented, pre-existing fracture, arrested soon after its nucleation. The arrest may happen due to the physical barriers to rupture propagation presented, for example, by the limited extent of the

pre-existing discontinuity, suggesting the minimum rupture area $\sim 4a_c^2 \sim 1$ m^2. If a typical stress drop of 3 MPa is employed, the calculated moment magnitude [*Hanks and Kanamori*, 1979] of the smallest earthquake is $M_w \approx -1.6$ (± 1.7), where the spread corresponds to the possible range of w and, therefore, of a_w. This magnitude range is consistent with the typical measured microseismicity induced by hydraulic fracturing [*Rutledge et al.*, 2004].

[73] Many well-studied mature fault zones are not favorably oriented to the existing stress field, and, therefore, operate at low background shear stress. For example, *Townend and Zoback* [2004] estimate from in-situ stress measurements $\tau^b/\overline{\sigma}_0 \sim 0.06 - 0.3$ for the San Andreas fault (SAF). Similarly, *Brune et al.* [1969] and *Lachenbruch and Sass* [1980] suggest $\tau^b/\overline{\sigma}_0 \lesssim 0.1$ to explain the lack of a detectable heat flow anomaly. This implies higher overpressure to activate the fault slip, and a nucleation patch size roughly 3 to 10 times larger than the above estimates for the critically stressed fractures in the crust. For example, $\tau^b/\overline{\sigma}_0 = 0.2$ and, as before, $a_w = 0.9$ m, give the nucleation patch $2a_c \approx 4.4$ m.

[74] Note that in many cases in this paper we normalize quantities of the length dimension by a_w. Therefore, for $a_w \simeq 1$ m, the corresponding dimensionless results (and plots) can be viewed as dimensional, expressed in meters.

[75] The run-out distance of seismic events on unfavorably oriented ($\tau^b < \tau_r$) but extensive (large) fractures or faults is likely to be constrained by the limited nature of the friction slip-weakening (rather than by physical barriers such as fracture "tips", intersections, etc.), unless the events become large enough to activate other (dynamic) weakening mechanisms, which can allow an entire fault or a large fault segment to rupture. For laboratory shear fracture of initially intact granite, the slip weakening distance is approximately $\delta_r \approx 0.5$ mm [*Rice*, 1980; *Wong*, 1986; *Uenishi and Rice*, 2003], and the corresponding ratio of residual-to-peak friction is $f_r/f_p = 1 - \delta_r/\delta_w \approx 0.6$, where, as before, $\delta_w \approx 1.2$ mm. Examples of numerical calculations with $f_r/f_p = 0.6$ (Figures 10b and 10c) and the s.s.y. analysis (section 5.2 and Figure S3a in the auxiliary material) suggest that the dynamic run-out distance can vary between the order of nucleation size $2a_c$ to length scale $2\sqrt{\alpha t_c}$ of the pressurized region. The latter is at its maximum when the conditions of the marginal pressurization are approached. This may happen when a process with pore pressure slowly increasing up to and above the minimum value required to activate the slip (equation (6)) is realized. Considering, for example, marginal pressurization with overpressure 5% above the minimum slip-activation value, we estimate from (17) that $\sqrt{\alpha t_c} \approx 10 a_c$. Thus, for the nucleation size of $2a_c \approx 4.4$ m estimated above, the run-out distance may vary, depending on the pressurization conditions, between roughly 4.4 and 44 m. The corresponding moment magnitude varies between -0.4 and 1.6, although a wider range of $M_w \approx -2$ to 3 is also plausible for the possible range of the rate-weakening w values.

7.3. Time to Instability

[76] Permeability of the fractured fault rocks and gouge constituting a major fault zone varies over many orders of magnitude. For example, according to *Wibberley and Shimamoto* [2003] for the Medium Tectonic Line fault, $k \sim 10^{-19} - 10^{-15}$ m^2 at $\overline{\sigma}_o \sim 50$ MPa. Here, lower values are characteristic of both the centimeters-thick central ultracataclastic gouge layer, which accommodates the majority of slip, and undamaged rock, which is typically 10s to 100s of meters away from the fault [e.g., *Chester et al.*, 1993]. Higher values of this permeability range represent the foliated gouges and highly fractured rock at intermediate distances. It is plausible to assume that it is the higher values of the permeability spectrum that control fluid transport along the fault (if the source of fluid overpressure is within the damaged zone of the fault). Therefore, taking $k \approx 10^{-16}$ m^2, pore space expansivity $\beta_n \sim 10$/GPa [e.g., *Wibberley*, 2002], pore fluid compressibility $\beta_f \sim 1$/GPa, porosity $n = 0.05$, and fluid viscosity $\eta \sim 10^{-3}$ Pa · s, we estimate along-the-fault diffusivity $\alpha = (k/\eta)/(n(\beta_f + \beta_n))$ [e.g., *Rice*, 2006] as $\sim 10^{-3}$ m^2/s. The corresponding characteristic diffusion timescale is $t_w = a_w^2/\alpha \approx 15$ min when $a_w \approx 1$ m, but may vary by an order of magnitude (plus or minus) for the possible range of a_w.

[77] The time to instability t_c roughly scales with t_w for the intermediate values of understress $\tau_p - \tau^b$ (Figures 8c and 8d). However, $t_c \ll t_w$ for the critically stressed ($\tau^b \approx \tau_p$) and $t_c \gg t_w$ for the marginally pressurized ($f_p \Delta p \approx \tau_p - \tau^b$) end-member cases. Therefore, the favorably oriented, critically stressed fractures nucleate dynamic slip on a timescale less than a minute, while the unfavorably oriented, understressed faults may take hours and days to nucleate even when the source of the overpressure is in the close vicinity of the principal slip plane.

7.4. Injection-Induced Seismicity

[78] The discussed mechanisms for nucleating and sustaining dynamic slip due to local pore pressure increase in the crust may indicate the following pattern for injection-induced seismicity in the vicinity of a large fault.

[79] Pore fluid pressure increase due to the injection may first activate slip on favorably oriented (possibly critically stressed) fractures which are likely to be prolific within the wide damage zone associated with a well-developed fault. This initially stable slip may transition into dynamic one, but be promptly arrested at the pre-existing fracture tips leading to contained microseismicity spreading along the fault with the pore fluid diffusion front.

[80] Larger pore fluid overpressure is required to activate slip on a less favorably oriented principal fault plane. If the pore pressure is to increase continuously to a point of activating slip on the principal fault plane, the corresponding nucleation condition is that of a marginally pressurized fault. This nucleation condition can eventually be reached if pressurization is maintained over the required large nucleation time and the overpressure margin is sufficient to overcome natural variations of the local prestress and strength (which can otherwise precipitate earlier arrest of dynamic rupture). This results in potentially the largest dynamic slip run-out distances. As discussed in section 6, the nucleation under marginally pressurized conditions (on unfavorably oriented, but well-developed fault plane) and the associated large run-out distance may lead to the activation of dynamic weakening mechanisms and to the unabated rupture propagation spanning a large fault segment.

[81] The outlined process of seismicity development may have two distinct observables. First, we expect the change of the focal mechanism between the favorably oriented fractures (e.g., in the damage zone adjacent to the fault)

and unfavorably oriented fault (principal) slip surface. Consequently, there may be an increase in the event magnitudes associated with the mechanism change. This may signal nucleation on less-favorably oriented, but much better developed (extended) fault planes. The Denver injection-induced seismicity of 1962–68 [*Healy et al.*, 1968; *Hsieh and Bredehoeft*, 1981] may provide an example of such a focal mechanism change. Specifically, *Healy et al.* [1968] inferred the right-lateral strike-slip mechanism for microseismicity recorded by a dense seismic station network during two months in 1966, just before the injection was permanently ended. Three large shocks with magnitude 5+ that shook the Denver area more than a year later were studied by *Herrmann et al.* [1981], who concluded that these were dip-slip events on a normal fault dipping at about 55°. The two disparate focal mechanisms (strike-slip microseismicity and dip-slip earthquakes) inferred in these two studies may be reconciled within the framework of injection-induced seismicity developing in the vicinity of a large fault as suggested above.

[82] Second, due to the effect of dynamic weakening, we also expect the possible lack of intermediate size events, which may manifest itself as a gap in the earthquake magnitude range. For example, *Healy et al.* [1968] reported an order of magnitude gap between small and large earthquakes in the case of Denver seismicity. In less restrictive terms, there may be a deficiency of an intermediate magnitude range in the frequency-magnitude relation as, for instance, was observed in the case of Basel seismicity induced during stimulation of a geothermal reservoir [e.g., *Deichmann and Giardini*, 2009]. In general, the lower bound of the magnitude deficiency range may correspond to the maximum run-out distance on a marginally pressurized fault plane that has not yet resulted in the activation of the dynamic weakening, capable of sustaining seismic slip.

8. Conclusions

[83] We have studied nucleation and arrest of the dynamic slip on a pressurized, slip-weakening fault in a uniform background stress field. The pressurization takes place from a fluid source and leads to the activation of slip over a patch on the fault. We made a number of simplifying assumptions regarding (1) fluid source and fault loading, which allowed us to treat the slipping patch as a 2-D (mode II or III) crack, (2) nature of the weakening of the fault gouge, (3) homogeneity of the fault gouge properties and stress along the fault, and (4) negligible poroelastic and inelastic effects such as gouge dilatancy and change of the fluid transport properties of the gouge with the slip. These assumptions may warrant revisiting the results of this study within a more complete model. However, albeit these simplifications, the model captures the essential interplay between the deformation, fluid flow, and fault slip as it may lead to the development of the dynamic slip nucleation. Specifically, we show how the initially quasi-static expansion of the slipping patch, paced by the along-the-fault diffusion, may eventually lead to the instability and transition into dynamic rupture due to the slip-weakening nature of the fault friction. Furthermore, depending on the loading conditions, overpressure, and residual level of the fault strength, the dynamic slip can be potentially arrested, with the possibility to be renucleated again at a greater scale. Figure 11 shows a map of slip regimes in the space of these parameters.

[84] We provide a framework for analysis of the stated problem, which builds on the methodology of *Uenishi and Rice* [2003], used by these authors to study the instability on dry or drained slip-weakening faults. A similar approach has been recently used in the independent study of a problem of slip nucleation due to a locally elevated pore pressure in relation to landsliding [*Viesca and Rice*, 2012]. In this work, we provide a solution not limited to a particular injection scenario, to a permeability contrast between a fault and a host rock, or to the location of a fluid source (on or off the fault plane), in the two limiting cases of the fault loading, corresponding to the *critically loaded* and *marginally pressurized* faults. Prestress on a critically loaded fault is close to the static failure condition and only a small (spatially and magnitude-wise) pressure perturbation is required to activate the fault slip. In the case of marginally pressurized faults, when locally peaked fluid overpressure is just enough to activate the slip, prolonged injection time is required to reach the dynamic instability (nucleation of dynamic slip). These asymptotic end-members provide bounds to the general solution, obtained numerically for a particular injection scenario corresponding to the fluid source on the fault (characterized by the elevated permeability compared to the host rock and by either constant overpressure or constant flow rate conditions). Our main results are recounted below.

[85] 1. Fault is ultimately unstable when background shear stress exceeds the residual static strength ($\tau^b > \tau_r$).

[86] 2. Size of the dynamic nucleation patch is weakly dependent on fluid overpressure. It scales with the *Uenishi and Rice* [2003] length scale a_w (equation (11)) with the prefactor $\propto \tau_p/\tau^b$, and, therefore, only mildly depends on the prestress τ^b (regimes 2a and 2c in Figure 11). The situation is different when τ^b is just slightly larger than the residual strength τ_r (i.e., near the transition from the ultimately unstable to the stable fault-loading). In this case, the (re-) nucleation patch increases strongly with diminishing τ^b and becomes unbounded ($\propto a_w(\tau_p - \tau_r)^2/(\tau^b - \tau_r)^2$) with τ^b approaching τ_r. The latter behavior is a subset of regimes 2b and 3 in Figure 11 (adjacent to their vertical boundary), where the (re-) nucleation process is affected by the fault residual strength.

[87] 3. No dynamic slip nucleation is observed on the ultimately stable faults ($\tau^b < \tau_r$) for large fluid overpressure and intermediate values of the fault understress, that is, away from the two end-member cases of the critically loaded (small understress) and marginally pressurized fault, respectively (regime 4 in Figure 11). This is a consequence of the fact that for a large overpressure (bounded in this study by the value of the fault-normal stress), larger slip is expected earlier, in the quasi-static patch development, resulting in the fault friction reaching its residual value prior to the instability.

[88] 4. Furthermore, the stabilizing effect of increasing overpressure is maximized in the limit of incipient hydraulic fracturing (i.e., when the overpressure at the fluid source is equal to the ambient effective stress normal to the fault). In this limit, the instability is suppressed entirely on ultimately stable faults.

[89] 5. For moderate values of fluid overpressure that are still sufficient to activate the slip, even the ultimately stable

faults undergo a temporal episode of dynamic slip (regime 2c in Figure 11).

[90] 6. Although counterintuitive, the dynamic run-out distance and accumulated slip are the largest for the lowest value of fluid overpressure that can still activate the fault slip on marginally pressurized faults.

[91] 7. Marginally pressurized faults are the most vulnerable to the activation of dynamic weakening mechanisms (such as thermal pressurization or flash heating on asperities) capable of sustaining the earthquake slip, once nucleated. This is consistent with observations that largest injection-induced seismic events occur well after the end of injection [e.g., *Healy et al.*, 1968].

[92] 8. On the other hand, slip on marginally pressurized faults is expected to be the most sensitive to natural variations of the local prestress and fault strength. Such variation may precipitate earlier arrest of dynamic rupture. Placing further constraints on dynamic rupture arrest has to include characteristics of the fault prestress and strength heterogeneity [e.g., *Ampuero et al.*, 2006].

[93] 9. Finally, it is important to stress again the existence of a range of parameters (e.g., regions 2a, 2b, and 3 in Figure 11) for which the run-out distance of dynamic rupture can be theoretically unlimited or, in practice, very large. Since the large run-out distance may result in a large (and delayed) earthquake, one may want to keep this in mind during manipulations with subsurface fluids such as geothermal energy recovery, hydraulic fracturing, geological (CO_2) sequestration, and deep mining and petroleum operations. Because locations of mature faults are often unknown even in well-developed provinces, extensive geological reconnaissance is of utmost significance to support case-specific analyses based on this work or on another theoretical framework.

Appendix A: Scaling and Numerical Methods

[94] Using τ_p and δ_w to normalize the stress and the slip, respectively, we rewrite the condition of elastic equilibrium (1) in the normalized form

$$\frac{\tau(x)-\tau^b}{\tau_p} = -\frac{1}{2\pi(a/a_w)}\int_{-1}^{1}\frac{d\delta(as+x_0)/\delta_w}{ds}\frac{ds}{(x-x_0)/a-s}, \tag{A1}$$

where $a = (a_+ - a_-)/2$ and $x_0 = (a_+ + a_-)/2$. In view of the fault strength expression (4), the normalized elastic stress perturbation along the crack can be expressed as

$$\frac{\tau(x)-\tau^b}{\tau_p} = \frac{\tau_p-\tau^b}{\tau_p} - \left(1-\frac{f(\delta(x))}{f_p}\right) - \frac{f(\delta(x))}{f_p}\frac{p(x)-p_o}{\overline{\sigma}_o}. \tag{A2}$$

For the linear slip-weakening friction law (5), $f(\delta)/f_p = 1 - \delta/\delta_w$ in (A2). In the case of a symmetric crack, $x_0 = 0$, the equations (A1) and (A2) together with the first slip-rate finiteness condition in (2), govern the solution for the normalized slip δ/δ_w, stress τ/τ_p, and the crack length $2a/a_w$. These quantities are functions of the normalized coordinate $X = x/a$ (for slip and stress distributions), the fault understress parameter $(\tau_p - \tau^b)/\tau_p$, and two parameters, which define the normalized pore pressure distribution (7), namely, the normalized overpressure at the crack center $\Delta p/\overline{\sigma}_o$ and the normalized position of the diffusion "front" $\sqrt{\alpha t}/a_w$. For a general case of a non-symmetric crack, $X = (x - x_0)/a$, and (2b) provides an additional constraint to solve for an additional unknown x_0/a.

[95] In order to solve the system of equations (A1), (A2), and (2), we use two alternative numerical approaches, which are standard in problems involving singular Cauchy integrals [e.g., *Uenishi and Rice*, 2003; *Viesca and Rice*, 2012; *Garagash*, 2012]. These approaches are summarized below, as applied to problems considered in this work.

A1. Chebyshev Polynomial Representation

[96] This method relies on the expansion of the slip distribution into a series of the Chebyshev's polynomials [e.g., *Erdogan et al.*, 1973]

$$\frac{\delta(x)}{\delta_w} = \sum_{n=1}^{\infty} B_n \sin n\theta, \qquad \theta \equiv \arccos\frac{x-x_0}{a}, \tag{A3}$$

where B_n are arbitrary expansion coefficients. Substitution of (A3) in (A1) yields an expression for the stress perturbation,

$$\frac{\tau(x)-\tau^b}{\tau_p} = -\frac{1}{2a/a_w}\sum_{n=1}^{\infty} nB_n\frac{\sin n\theta}{\sin\theta}, \tag{A4}$$

which is then used to satisfy the finiteness conditions (2):

$$\sum_{n=1,3,5,\ldots}^{\infty} nB_n = 0, \qquad \sum_{n=2,4,6,\ldots}^{\infty} nB_n = 0. \tag{A5}$$

[97] An approximate solution is obtained by truncating the above series to the first N terms. Equating expressions for the stress perturbation resulting from (A2) with (A3) and from (A4) at the N collocation points $\theta(x_k) = (\pi/2)(2k-1)/N$ ($k = 1, \ldots, N$) along the crack, $(x_k - x_0)/a \in (1, -1)$, yields a system of algebraic equations for B_i ($i = 1, \ldots, N$). The latter, together with the two slip-rate finiteness conditions (A5), results in the system of $N + 2$ equations for $N + 2$ unknowns a/a_w, x_0/a, and coefficients $B_{1,\ldots,N}$.

[98] For a symmetric crack, $x_0/a = 0$ and the even-numbered terms in (A3) are nil, i.e., $B_{2,4,6\ldots} = 0$ and (A5b) is automatically satisfied. In this case, an odd N and the first $(N + 1)/2$ collocation points along the positive half of the crack, $x/a \in (1, 0]$, are used to evaluate the elasticity equation (A2) with (A4). The resulting system of $(N + 3)/2$ algebraic equations together with the non-trivial finiteness condition (A5a) is solved for a/a_w and the $(N + 1)/2$ odd-numbered coefficients $B_{1,3,5,\ldots,N}$. Results reported in this work have been obtained using $N = 100$ expansion terms.

A2. Piecewise Constant Slip Method

[99] In this method, the slip is approximated by a piecewise constant distribution over $2N$ uniformly spaced elements ($\Delta X = 1/N$) with midpoints $X_j = j\Delta X$ ($j = -N, \ldots, N$), where, as already defined before, $X = (x - x_0)/a \in [-1, 1]$ is the normalized coordinate along the crack. This discretization leads to the well-known approximation for the elastic stress perturbation (A1) at the grid points [e.g., *Uenishi and Rice*, 2003]:

$$\frac{\tau(i\Delta X)-\tau^b}{\tau_p} = -\frac{a_w}{a}\sum_j K_{ij}\frac{\delta(j\Delta X)}{\delta_w}, \tag{A6}$$

where $K_{ij} = -1/(2\pi\Delta X[(i-j)^2 - 1/4])$ and $\delta(\pm N\Delta X) = 0$. Note that the stress and slip in (A6) are expressed in terms of the normalized coordinate X rather than the dimensional x in the original equation (A1). Equating (A6) evaluated at the interior grid points ($-N < i < N$) to the corresponding expressions from the constitutive law (A2) yields $2N-2$ algebraic equations on the same number of the slip unknowns. Solution of this set depends on the crack length a, eccentricity x_0, and the background stress τ^b. Quantities a and x_0 are related to τ^b by the finiteness conditions (2). In the case of the symmetric crack, $x_0 = 0$, and the relevant finiteness condition (the first in (2)) is evaluated using (A2) and the slip discretization as follows:

$$\frac{\tau^b}{\tau_p} = \sum_j k_j \frac{f(\delta(j\Delta X))}{f_p},$$

where

$$k_j = \frac{1}{\pi} \int_{\max\{-1,(j-0.5)\Delta X\}}^{\min\{+1,(j+0.5)\Delta X\}} \left(1 - \frac{p(aX,t) - p_o}{\overline{\sigma}_o}\right) \frac{dX}{\sqrt{1-X^2}}.$$

[100] When using the above numerical scheme to solve for the slip and the slipping patch length as a function of the background stress τ^b (and time t, which enters as a parameter in the pore pressure for a given injection scenario), we found it more convenient to specify the crack length (and time) and solve for τ^b and slip δ. Results reported in this paper have been obtained for $2N = 120$ discretization elements along the crack, which yields an accurate solution within the reported range of the normalized crack length and injection time. Comparison of the numerical results obtained by two different methods (i.e., by the polynomial expansion method described in section A1 and the discretization method discussed above) for the case of friction law with unlimited slip-weakening shows that the difference is practically negligible.

Appendix B: Asymptotics of Marginally Pressurized Fault ($f_p\Delta p \simeq \tau_p - \tau^b$) at Slip Instability

[101] As discussed in section 4.1, in this case, the normalized slip δ/δ_w is expected to be small, and so is the deviation of fluid pressure $p(x)$ along the crack from its value at the center $p_o + \Delta p$. In addition, $f(\delta)/f_p = 1 - \delta/\delta_w$ according to (5). Therefore, approximation $(f(\delta)/f_p)(p(x) - p_o) \simeq \Delta p - \Delta p(\delta/\delta_w) - (\Delta p - (p(x) - p_o))$ is valid and can be substituted into the expression (A2) for the normalized stress perturbation along the crack. After rearranging terms, we obtain

$$\frac{\tau(x) - \tau^b}{\tau_p} = -\frac{f_p\Delta p - (\tau_p - \tau^b)}{\tau_p} - \left(1 - \frac{\Delta p}{\overline{\sigma}_o}\right)\frac{\delta(x)}{\delta_w} + \frac{\Delta p - (p(x) - p_o)}{\overline{\sigma}_o}. \quad \text{(B1)}$$

The first term $\tilde{\epsilon} = (f_p\Delta p - (\tau_p - \tau^b))/\tau^b$ in the right hand side is a small dimensionless parameter, which scales other terms in (B1), including the normalized stress perturbation in the left hand side. Equating (B1) to the elasticity integral (A1) with the crack length asymptote (16), and dividing the result by $\tilde{\epsilon}$, we obtain

$$\frac{\tau(x) - \tau^b}{\tilde{\epsilon}\tau^b} = -1 - \frac{\delta(x)}{\tilde{\epsilon}\delta_w} + F(x/a) = -\frac{1}{(2\pi)a/a_w}\int_{-1}^{1} \frac{d\delta(as)/(\tilde{\epsilon}\delta_w)}{ds}\frac{ds}{x/a - s}, \quad \text{(B2)}$$

where $F(x/a)$ is the scaled pressure drop along the crack, which, in view of the near-uniformity of the pressure along the crack, can be further approximated by the Taylor series expansion at the crack center:

$$F(x/a) \equiv \frac{f_p\Delta p}{f_p\Delta p - (\tau_p - \tau^b)}\left(1 - \frac{p(x) - p_o}{\Delta p}\right) \simeq A_1\frac{|x|}{a} + A_2\frac{x^2}{a^2}. \quad \text{(B3)}$$

Here Taylor coefficients

$$A_{1,2} = \frac{f_p}{f_p\Delta p - (\tau_p - \tau^b)}\left\{a\left|\frac{dp}{dx}\right|, -\frac{a^2}{2}\frac{d^2p}{dx^2}\right\}_{x=0}, \quad \text{(B4)}$$

and only the first non-zero term is to be considered in expansion (B3). The linear term is non-zero when, for example, the fluid is injected into a transversely impermeable fault zone (e.g., equation (7) with (8) or (9)) and the quadratic term is negligible. On the other hand, the linear term is null when the pressure profile is smooth at the crack center (i.e., $(dp/dx)_{x=0} = 0$), such as the case of fluid injection at a distance from the fault plane (equations (7) and (10)).

[102] Equations (B2) and (B3) together with the appropriately normalized first finiteness condition in (2) are solved for the scaled slip distribution $\delta(x)/(\tilde{\epsilon}\delta_w)$ and either A_1, when $(dp/dx)_{x=0} \neq 0$, or A_2, otherwise, using the Chebyshev polynomial representation method (described in section A1 for a similar problem) and considering the crack length a known. The two numerical solutions at nucleation ($a = a_c \simeq 0.579a_w$) for injection scenarios such as (8) (or (9)) and (10) are given by

$$A_1 \simeq 2.487, \quad A_2 \simeq 4.384, \quad \text{(B5)}$$

respectively, and the corresponding scaled slip distributions are shown in Figure 5. Depending on the injection scenario, the (large) nucleation time can be recovered from the relevant expression in (B4), as further discussed in the main text.

Appendix C: Asymptotics of Critically Loaded Fault ($\tau^b \simeq \tau_p$) at Slip Instability

C1. Outer Solution ($x \gg \sqrt{\alpha t}$)

[103] In this case, the extent of the pressurized region is much smaller than the extent of the quasi-statically slipping crack, $\sqrt{\alpha t} \ll a$, and the pressure distribution can be effectively replaced by the equivalent "point-force" distribution

$$p(x,t) - p_o \simeq \Delta P(t)\delta_{Dirac}(x) \quad \left(x \gg \sqrt{\alpha t}\right), \quad \text{(C1)}$$

where $\delta_{Dirac}(x)$ is the Dirac delta function and $\Delta P(t) = \int_{-\infty}^{\infty}(p(x,t) - p_o)dx$.

[104] The normalized perturbations of stress, $(\tau - \tau^b)/\tau_p$, slip, δ/δ_w, and pore pressure, $(p - p_o)/\overline{\sigma}_0$, are small, and, in view of (A1) and (A2), scale with the normalized understress

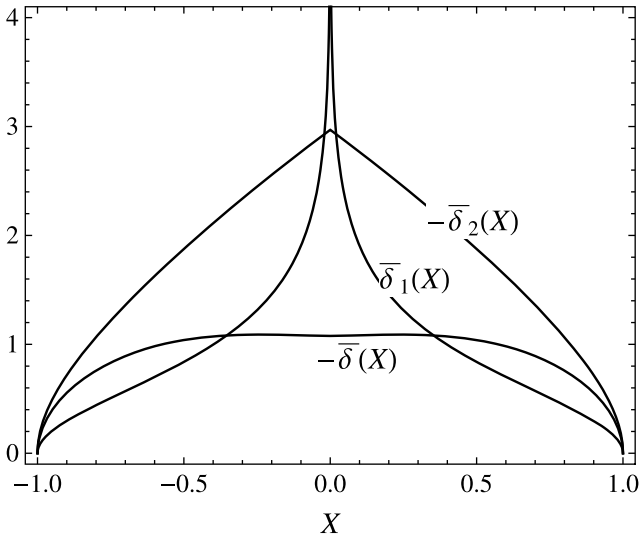

Figure C1. Terms in the outer solution $\delta(aX)/\epsilon\delta_w = \mathcal{P}(\overline{\delta}_1(X) - (a/a_w)\overline{\delta}_2(X)) + \overline{\delta}(X)$ (equation (C6)), for critically loaded faults ($\epsilon = 1 - \tau^b/\tau_p \ll 1$) at the instability ($a = a_c \simeq 0.579a_w$ and $\mathcal{P} \simeq 0.8369$).

parameter $\epsilon = 1 - \tau^b/\tau_p \ll 1$. Retaining the leading, $O(\epsilon)$ terms in (A2),

$$\frac{\tau(x) - \tau^b}{\tau_p} = \epsilon - \frac{\delta(x)}{\delta_w} - \frac{p(x) - p_o}{\overline{\sigma}_o} + O(\epsilon^2), \tag{C2}$$

and substituting the result, together with expression (C1) for the pore pressure, in the left hand side of (A1), yields

$$\frac{a}{a_w}\left(1 - \frac{\delta(x)}{\epsilon\delta_w}\right) - \mathcal{P}\delta_{Dirac}(x/a) = -\frac{1}{2\pi}\int_{-1}^{1} \frac{d\delta(as)/(\epsilon\delta_w)}{ds}\frac{ds}{x/a - s}, \tag{C3}$$

where we used the scaling property of $\delta_{Dirac}(x)$,

$$\mathcal{P} = \frac{\Delta P}{\epsilon a_w \overline{\sigma}_0} = \frac{\Delta p}{\overline{\sigma}_0}\frac{\sqrt{\alpha t}}{\epsilon a_w}\int_{-\infty}^{\infty} \Pi(\xi)d\xi \tag{C4}$$

is the scaled magnitude of the "point" force, $\Pi(\xi)$ corresponds to a particular class (7) of pressure distributions, and $\Delta P/(\overline{\sigma}_0 a_w) \sim \epsilon$. Similarly, the first condition in (2) of the finiteness of the slip rate at the tips of a symmetric crack can then be reduced to

$$\frac{a}{a_w}\left(1 - \frac{1}{\pi}\int_{-1}^{1} \frac{\delta(aX)/(\epsilon\delta_w)}{\sqrt{1 - X^2}}dX\right) - \frac{1}{\pi}\mathcal{P} = 0. \tag{C5}$$

[105] Let us denote the normalized integral operator in the right hand side of (C3) and its inverse as

$$\mathcal{L}[f](X) \equiv -\frac{1}{2\pi}\int_{-1}^{1} \frac{df(s)}{ds}\frac{ds}{X - s},$$
$$\mathcal{L}^{-1}[F](X) = \frac{2}{\pi}\int_{-1}^{1} \ln\left|\frac{X - s}{1 - sX + \sqrt{1 - s^2}\sqrt{1 - X^2}}\right| F(s)ds,$$

respectively, where the expression for $\mathcal{L}^{-1}$ is obtained by integrating in X the classic inversion of the Cauchy integral over a finite interval of the real axis [*Muskhelishvili*, 1977]. We look for the solution of (C3) and (C5) for the normalized slip distribution in the form of

$$\frac{\delta(aX)}{\epsilon\delta_w} = \mathcal{P}\left(\overline{\delta}_1(X) - \frac{a}{a_w}\overline{\delta}_2(X)\right) + \overline{\delta}(X), \tag{C6}$$

where $\overline{\delta}_1 \equiv \mathcal{L}^{-1}[-\delta_{Dirac}]$, $\overline{\delta}_2 \equiv \mathcal{L}^{-1}[\overline{\delta}_1]$, and $\overline{\delta}$ is an auxiliary unknown function continuous and differentiable for all $X \in (-1, 1)$. This function satisfies (C3) and (C5), which can be written in the form of

$$\frac{a}{a_w}\left(1 + \mathcal{P}\frac{a}{a_w}\overline{\delta}_2(X) - \overline{\delta}(X)\right) = \mathcal{L}[\overline{\delta}](X) \tag{C7}$$

$$\frac{a}{a_w}\left(1 - \mathcal{P}\left(\mathcal{K}[\overline{\delta}_1] - \frac{a}{a_w}\mathcal{K}[\overline{\delta}_2]\right) - \mathcal{K}[\overline{\delta}]\right) - \frac{1}{\pi}\mathcal{P} = 0, \tag{C8}$$

respectively, $\mathcal{K}[\overline{\delta}] \equiv \frac{1}{\pi}\int_{-1}^{1}(\overline{\delta}(X/\sqrt{1 - X^2})dX$. Functions $\overline{\delta}_1(X)$ and $\overline{\delta}_2(X)$ are evaluated analytically,

$$\overline{\delta}_1(X) = \frac{2}{\pi}\ \mathrm{In}\left(\left(1 + \sqrt{1 - X^2}\right)/|X|\right),$$

and numerically, respectively, and plotted in Figure C1. Numerical values of the corresponding terms in (C8) are $\mathcal{K}[\overline{\delta}_1] \simeq 0.7425$ and $\mathcal{K}[\overline{\delta}_2] \simeq -1.3942$.

[106] In order to find the numerical solution for $\overline{\delta}(X)$ and $\mathcal{P}$, we use the Chebyshev polynomial representation,

$$\overline{\delta}(X) = \sum_{n=1}^{\infty} B_n \sin n\theta, \quad \mathcal{L}[\overline{\delta}](X) = -\frac{1}{2}\sum_{n=1}^{\infty} nB_n \frac{\sin n\theta}{\sin\theta}$$
$$(\theta = \arccos X), \tag{C9}$$

$\mathcal{K}[\overline{\delta}] = \frac{2}{\pi}\sum_{n=1}^{\infty} B_n/n$ with $B_{2,4,6,\ldots} = 0$, truncated to the first odd N terms, to evaluate (C8) and (C7) at $(N + 1)/2$ collocation points defined in section A1. For a given patch size, a, the resulting system of $(N + 1)/2 + 1$ algebraic equations is solved for $(N + 1)/2$ odd-numbered coefficients $B_{1,3,5,\ldots,N}$ and $\mathcal{P}$. At the instability, $a = a_c \simeq 0.579a_w$ (equation (16)).

[107] The numerical solution is given by

$$\mathcal{P} \simeq 0.8369 \quad (a = a_c) \tag{C10}$$

and distribution $\overline{\delta}(X)$ shown in Figure C1 for $a = a_c$. We note that the first three, non-zero terms of the slip series expansion (C9),

$$\overline{\delta}(X) \approx B_1 \sin\theta(X) + B_3 \sin 3\theta(X) + B_5 \sin 5\theta(X),$$

where $B_1 = -1.1732$, $B_3 = -0.0608$, and $B_5 = 0.0235$, provide an excellent approximation (1% error or less) to the solution for $a = a_c$.

[108] We also note that the complete outer solution (C6) has a non-physical, logarithmic singularity at the crack center because the pressure distribution was replaced there by a point force. Specifically, the following near-field asymptotic expansion of (C6) is valid at $X = x/a \ll 1$ and $a = a_c$:

$$\frac{\delta(x)}{\epsilon\delta_w} = -\frac{2}{\pi}\mathcal{P}\ln\frac{|X|}{2} - \frac{a}{a_w}\mathcal{P}\overline{\delta}_2(0) + \overline{\delta}(0) + O(X), \tag{C11}$$

where $\mathcal{P} \simeq 0.8369$, $a/a_w \simeq 0.579$, $\overline{\delta}_2(0) \simeq -2.970$, and $\overline{\delta}(0) \simeq -1.077$. Below, we explicitly consider the nature of

the slip solution within the small pressurized region near the crack center.

C2. Inner Solution ($x \sim \sqrt{\alpha t}$)

[109] Normalized pressure perturbation $(p(x) - p_o)/\overline{\sigma}_o \sim 1$ within a small pressurized region $x \sim \sqrt{\alpha t}$ near the crack center. In this region, expression (A2) for the stress perturbation can be approximated as

$$\frac{\tau(x) - \tau^b}{\tau_p} = -\frac{p(x) - p_o}{\overline{\sigma}_o} + O(\epsilon) \quad \left(\epsilon = 1 - \frac{\tau^b}{\tau_p} \ll 1\right). \quad \text{(C12)}$$

On the other hand, the elasticity equation (A1) can be rewritten as

$$\frac{\tau(x) - \tau^b}{\tau_p} = -\frac{1}{2\pi}\frac{\epsilon a_w}{\sqrt{\alpha t}}\int_{-a/\sqrt{\alpha t}}^{a/\sqrt{\alpha t}} \frac{d\delta\left(\sqrt{\alpha t}s\right)/\epsilon\delta_w}{ds}\frac{ds}{x/\sqrt{\alpha t} - s}. \quad \text{(C13)}$$

Equating (C12) and (C13), using pressure distribution in the form of (7), expressing $\sqrt{\alpha t}$ from (C4), and passing to the limit of $a/\sqrt{\alpha t} \to \infty$ results, after some simplification, in equation

$$\frac{\Pi(\xi)}{\int_{-\infty}^{\infty}\Pi(s)ds} = \frac{1}{2\pi\mathcal{P}}\int_{-\infty}^{\infty}\frac{d\hat{\delta}(s)}{ds}\frac{ds}{\xi - s}, \quad \text{(C14)}$$

where both right and left hand sides are of the $O(1)$, $\hat{\delta}(\xi) = \delta(\sqrt{\alpha t}\xi)/\epsilon\delta_w$ is the normalized slip in the inner solution, and $\xi = x/\sqrt{\alpha t}$ is the normalized coordinate. Solution of (C14) for the normalized slip rate is given by the inverse Hilbert transform [e.g., *King*, 2009], which, upon further integration for the slip, becomes

$$\hat{\delta}(\xi) = \hat{\delta}(0) - \frac{2}{\pi}\mathcal{P}\frac{\int_{-\infty}^{\infty}\Pi(s)\ln|1 - \xi/s|ds}{\int_{-\infty}^{\infty}\Pi(s)ds}. \quad \text{(C15)}$$

C3. Matching Outer and Inner Solutions

[110] In order to find the unknown normalized slip at the center, $\hat{\delta}(0) = \delta_{|x=0}/\epsilon\delta_w$, we use the method of matched asymptotics [e.g., *Kevorkian and Cole*, 1996]. Specifically, we match the inner and outer solutions at the intermediate distances from the crack center. To characterize behavior of the inner solution (C15) in the far field $\xi = x/\sqrt{\alpha t} \gg 1$, we rewrite (C15) as

$$\frac{\delta(x)}{\epsilon\delta_w} \simeq \hat{\delta}(0) - \frac{2}{\pi}\mathcal{P}\ln|\xi| + \frac{2}{\pi}\mathcal{P}\frac{\int_{-\infty}^{\infty}\Pi(s)\ln|s|ds + I(\xi)}{\int_{-\infty}^{\infty}\Pi(s)ds}, \quad \text{(C16)}$$

where integral $I(\xi) = \int_{-\infty}^{\infty}\Pi(s)\ln|s/\xi - 1|ds$ vanishes for large ξ. To show this, consider, without a loss of generality, an even function $\Pi(\xi)$ with indefinite integral $F(\xi) = -\int_{\xi}^{\infty}\Pi(\xi)d\xi$. Then, $I(\xi) = \int_0^{\infty}\Pi(s)\ln|s^2/\xi^2 - 1|ds = -\int_0^{\infty}F(s)\frac{d(s^2)}{s^2 - \xi^2}$, where the last equality follows from the integration by parts and using $F(\infty) = 0$. Thus, $I(\xi)$ is a Cauchy integral on a semi-infinite interval, which is known to converge for any $F(\xi)$ vanishing (at least algebraically fast) as $\xi \to \infty$. Furthermore, asymptotic properties of this integral are such that if $F(\xi) \sim \xi^{-\gamma}$ $(\gamma > 0)$ as $\xi \to \infty$, then $I(\xi) \sim \xi^{-\gamma}$ in the same limit [e.g., *Garagash et al.*, 2011]. Thus, we maintain that integral $I(\xi)$ vanishes in the limit of large ξ for an arbitrary integrable distribution $\Pi(\xi)$ that decays at infinity at least as fast as $\Pi(\xi) \sim \xi^{-1-\gamma}$ $(\gamma > 0)$. Such a property certainly holds for pore pressure perturbations borne by linear diffusion and characterized by a faster-than-power law decay with distance from the source.

[111] Matching the near-field $(X \to 0)$ asymptotic expansion (C11) of the outer solution (C6) with the far field $(\xi \to \infty)$ expansion of the inner solution, which follows from (C16) by neglecting $I(\xi)$, at the intermediate distances $\sqrt{\alpha t} \ll x \ll a$ from the crack center to the $O(1)$ yields the asymptotic expression for the normalized slip at $x = 0$:

$$\frac{\delta_{|x=0}}{\epsilon\delta_w} = \mathcal{P}\left(-\frac{2}{\pi}\ln\frac{\sqrt{\alpha t}}{2a} - \frac{2}{\pi}\frac{\int_{-\infty}^{\infty}\Pi(s)\ln|s|ds}{\int_{-\infty}^{\infty}\Pi(s)ds} - \frac{a}{a_w}\overline{\delta}_2(0)\right) + \overline{\delta}(0). \quad \text{(C17)}$$

We finally make use of expression $\sqrt{\alpha t}/a = (a_w/a)(\mathcal{P}/\int_{-\infty}^{\infty}\Pi(s)ds)\hat{\epsilon}$, as follows from (C4), and relationship $\hat{\epsilon} \equiv (\Delta p/\overline{\sigma}_0)^{-1}\,\epsilon = (\tau_p - \tau^b)/f_p\Delta p$ between the inner and outer small parameters, to evaluate slip (C17) at the instability

$$\frac{\left(\delta_{|x=0}\right)_c}{\delta_w} = 0.533\epsilon\left(-\ln\frac{\hat{\epsilon}}{C} + 1.003\right)$$
$$\text{with} \quad C = \left(\int_{-\infty}^{\infty}\Pi(s)ds\right)\exp\left(-\frac{\int_{-\infty}^{\infty}\Pi(s)\ln|s|ds}{\int_{-\infty}^{\infty}\Pi(s)ds}\right). \quad \text{(C18)}$$

where the numerical values of $\mathcal{P}$, $\Delta p(t)$, a/a_w, $\overline{\delta}_2(0)$, and $\overline{\delta}(0)$ at the instability were utilized (section C1). The value of C depends upon the specific distribution $\Pi(s)$. For constant overpressure and constant injection rate, $\Pi(\xi)$ is given by (8) and (9), resulting in $C = 4.0935$ and $C = 3.9000$, respectively.

Appendix D: Improved S.S.Y. Asymptotics

[112] Consider an auxiliary problem of slip propagation on a uniformly loaded fault with limited slip-weakening and uniform pore pressure. This problem is mathematically identical to that of a cohesive crack with linear softening and propagating under uniform far-field tension in the "fixed-grip" conditions studied by *Dempsey et al.* [2010]. Let the size of the end zone be d and the length of the "traction-free" part of the crack $b = a - d$. *Dempsey et al.* [2010] found a numerical solution for the normalized length d/λ of the end

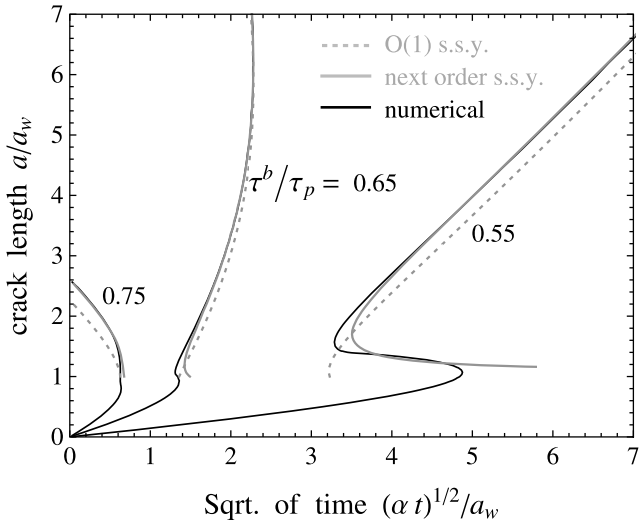

Figure D1. Comparison of the numerical solution with the zero-order s.s.y. (dotted, gray lines) and the next-order s.s.y. (using the "effective crack length" a_{eff}, equation (D2), solid gray lines) asymptotic solutions for development of the crack half-length at three values of the fault background stress τ^b/τ_p and the fixed fluid overpressure $\Delta p/\overline{\sigma}_o = 0.5$ at the crack center in the model with residual friction $f_r/f_p = 0.6$ (as in Figure 9b, left).

zone and the normalized loading $(\tau^b - \tau_r)/(\tau_p - \tau_r)$ as functions of the normalized length b/λ of the "traction-free" part of the crack (i.e., $\alpha - \beta$ and $\hat{\sigma}_\infty$, respectively, as functions of β in their notations shown in their Figure 3b), where $\lambda = (\pi/2)(K/(\tau_p - \tau_r))^2$ is a characteristic length scale. The large crack asymptote, $b/\lambda \gg 1$, is given by

$$d \simeq 0.466\lambda, \quad \tau^b - \tau_r \simeq \frac{K}{\sqrt{\pi b}}\left(1 - 0.1245\frac{\lambda}{b} + O\left(\frac{\lambda}{b}\right)^2\right), \tag{D1}$$

where $K = \sqrt{2\mu^* G_c}$ for a growing fracture. The first term in expansion (D1) is the s.s.y. asymptote, while the second term is the first-order correction. This expansion can be rewritten in a convenient form of

$$K = \left(\tau^b - \tau_r\right)\sqrt{\pi a_{\text{eff}}}, \quad a_{\text{eff}} \simeq b + 0.249\lambda \simeq a - 0.466d, \tag{D2}$$

which incorporates the next order correction to the s.s.y. asymptote $K = (\tau^b - \tau_r)\sqrt{\pi a}$.

[113] Based on this solution for the auxiliary problem, we observe that a more accurate result for the far-field stress intensity factor in the large crack limit can be obtained by reducing the crack length a in the corresponding s.s.y. expressions (such as (28) in the case of pore fluid pressurization) by a fraction of the end zone length. Specifically, as follows from (D2), a should be replaced with $a_{\text{eff}} \simeq a - 0.466d$. According to (D1a), the end zone length for the problem of interest is given by $d \simeq 0.466\lambda$, where length scale λ can be expressed, in view of (27) and (11), as $\lambda = (\pi/2)(\overline{\sigma}_o/\overline{\sigma}(a))a_w$. A comparison of the asymptotes using a and a_{eff} in the s.s.y. solution is given in Figure D1.

Appendix E: Asymptotics of Large Dynamic Run-Out

[114] When $a \gg a_w$, (28) suggests that to the first order, $\Delta K \simeq (\tau_r - \tau^b)\sqrt{\pi a}$ (because K is bounded in (28)). For the pore pressure perturbation in the form of (7), we find an implicit expression for the $O(1)$ approximation of the s.s.y. solution for the crack length (denoted here by $a^{(0)}$) as a fraction of the pressurized length scale:

$$\kappa\left(\frac{a^{(0)}}{\sqrt{\alpha t}}\right) = \frac{\tau_r - \tau^b}{f_r \Delta p}, \qquad \kappa(\xi) \equiv \frac{1}{\pi}\int_{-1}^{1} \frac{\Pi(\xi s)ds}{\sqrt{1-s^2}}, \tag{E1}$$

where function $\kappa(\xi)$ decreases from the $\sim$1 maximum value at $\xi = 0$ to zero at $\xi = \infty$.

[115] The corresponding, first-order approximation $\delta^{(0)}$ of the fault slip can be calculated from the classical inversion [*Rice*, 1968] of (1) using (4) with $f \approx f_r$ (since most of the surface of the large crack, $a \gg a_w$, is in the state of residual friction). In the case of pressure distribution (7), we use (E1) to obtain the peak slip at the crack center:

$$\left(\frac{\delta_{|x=0}}{a}\right)^{(0)} = \frac{f_r \Delta p}{\mu^*}\Omega\left(\frac{a^{(0)}}{\sqrt{\alpha t}}\right), \tag{E2}$$

where

$$\Omega(\xi) = \frac{2}{\pi}\int_{-1}^{1}\left\{\ln\left|\frac{\sqrt{1+s}+\sqrt{1-s}}{\sqrt{1+s}-\sqrt{1-s}}\right| - \frac{1}{\sqrt{1-s^2}}\right\}\Pi(\xi s)ds.$$

[116] The obtained equations provide asymptotic expressions for the length of the arrested dynamic rupture (equation (E1)) and the corresponding accumulated peak slip at the crack center (equation (E2)) for a marginally pressurized fault ($f_p \Delta p \simeq \tau_p - \tau^b$). In both (E1) and (E2), time $t = t_c$ is the nucleation time. For a particular pressurization scenario (7), characterized by a constant overpressure and along-the-fault diffusion, t_c is given by (17). For this scenario, the crack length and peak slip are exemplified in Figure S3 in the auxiliary material for various values of the residual-to-peak friction ratio f_r/f_p.

[117] Comparison of asymptote (E1) with the full s.s.y. solution for the arrested rupture size in Figure S4 in the auxiliary material shows that (E1) is an accurate approximation for very large size of the pressurized region $\sqrt{\alpha t}/a_w \gtrsim 10^3$ at the nucleation/arrest of the dynamic rupture driven by moderate overpressure. In other words, in view of (17), the fluid overpressure Δp has to be within 0.1% of the understress value at the slip activation, $(\tau_p - \tau^b)/f_p$, for the asymptote (E1) and (E2) to hold. For a less restrictive overpressure margin, the asymptotic expressions (E1) and (E2) are less accurate, yet provide an adequate order-of-magnitude estimate of the run-out distance of dynamic rupture and the associate fault slip. For example, $\Delta p = 1\%$ corresponds to about 20% error in the predicted arrested crack length (Figure S4 in the auxiliary material).

[118] **Acknowledgments.** Support for this research by the National Science Foundation (grants CMMI-0919497, EAR-1036985, OCE-1131355) and by the Natural Science and Engineering Research Council of Canada (Discovery grant 371606) is acknowledged. The paper was finalized during Dmitry Garagash's sabbatical stay at Harvard University, which support is also acknowledged. We are grateful to Jim Rice and Robert Viesca for discussions and thank two anonymous reviewers and the Associate Editor for helpful comments.

References

Abramowitz, M., and I. Stegun (Eds.) (1972), *Handbook of Mathematical Functions with Formulas, Graphs, and Mathematical Tables*, Dover, New York.

Ague, J. J., J. Park, and D. M. Rye (1998), Regional metamorphic dehydration and seismic hazard, *Geophys. Res. Lett.*, *25*(22), 4221–4224.

Ampuero, J.-P., and A. M. Rubin (2008), Earthquake nucleation on rate and state faults: Aging and slip laws, *J. Geophys. Res.*, *113*, B01302, doi:10.1029/2007JB005082.

Ampuero, J.-P., J. Ripperger, and P. M. Mai (2006), Properties of dynamic earthquake ruptures with heterogeneous stress drop, in *Earthquakes: Radiated Energy and the Physics of Faulting*, *Geophys. Monogr. Ser.*, vol. 170, edited by R. Abercrombie et al., pp. 255–261, AGU, Washington, D. C.

Andrews, D. J. (1976), Rupture propagation with finite stress in antiplane strain, *J. Geophys. Res.*, *81*(20), 3575–3582.

Andrews, D. J. (2002), A fault constitutive relation accounting for thermal pressurization of pore fluid, *J. Geophys. Res.*, *107*(B12), 2363, doi:10.1029/2002JB001942.

Beeler, N. M., T. E. Tullis, M. L. Blanpied, and J. D. Weeks (1996), Frictional beahavior of large displacement experiemental faults, *J. Geophys. Res.*, *101*, 8697–8715.

Beeler, N. M., T. E. Tullis, and D. L. Goldsby (2008), Constitutive relationships and physical basis of fault strength due to flash heating, *J. Geophys. Res.*, *113*, B01401, doi:10.1029/2007JB004988.

Bilby, B., and J. Eshelby (1968), Dislocations and the theory of fracture, in *Fracture, An Advanced Treatise*, vol. I, edited by H. Liebowitz, chap. 2, pp. 99–182, Academic, New York.

Bizzarri, A., and M. Cocco (2006a), A thermal pressurization model for the spontaneous dynamic rupture propagation on a three-dimensional fault: 1. Methodological approach, *J. Geophys. Res.*, *111*, B05303, doi:10.1029/2005JB003862.

Bizzarri, A., and M. Cocco (2006b), A thermal pressurization model for the spontaneous dynamic rupture propagation on a three-dimensional fault: 2. Traction evolution and dynamic parameters, *J. Geophys. Res.*, *111*, B05304, doi:10.1029/2005JB003864.

Brune, J. N., T. L. Henyey, and R. F. Roy (1969), Heat flow, stress, and rate of slip along the San Andreas fault, California, *J. Geophys. Res.*, *74*(15), 3821–3827.

Campillo, M., and I. R. Ionescu (1997), Initiation of antiplane shear instability under slip dependent friction, *J. Geophys. Res.*, *102*, 20,363–20,371.

Cappa, F., and J. Rutqvist (2011), Impact of CO2 geological sequestration on the nucleation of earthquakes, *Geophys. Res. Lett.*, *38*, L17313, doi:10.1029/2011GL048487.

Carslaw, H., and J. C. Jaeger (1959), *Conduction of Heat in Solids*, 2nd ed., Oxford Univ. Press, Oxford, U. K.

Chester, F. M., and J. S. Chester (1998), Ultracataclasite structure and friction processes of the Punchbowl fault, San Andreas system, California, *Tectonophysics*, *295*, 199–221.

Chester, F. M., J. P. Evans, and R. L. Biegel (1993), Internal structure and weakening mechanisms of the San Andreas fault, *J. Geophys. Res.*, *98*(B1), 771–786.

Chester, F. M., J. S. Chester, D. L. Kirschner, S. E. Schulz, and J. P. Evans (2004), Structure of large-displacement, strike-slip fault zones in the brittle continental crust, in *Rheology and Deformation in the Lithosphere at Continental Margins*, edited by G. D. Karner et al., pp. 199–221, Columbia Univ. Press, New York.

Cornet, F. H., J. Helm, H. Poitrenaud, and A. Etchecopar (1997), Seismic and aseismic slips induced by large-scale fluid injections, *Pure Appl. Geophys.*, *150*, 563–583.

Dascalu, C., I. R. Ionnescu, and M. Campillo (2000), Fault finiteness and initiation of dynamic shear instability, *Earth and Planet. Sci. Lett.*, *177*, 163–176.

Deichmann, N., and D. Giardini (2009), Earthquakes induced by the stimulation of an enhanced geothermal system below Basel (Switzerland), *Seismol. Res. Let.*, *80*(5), 784–798.

Dempsey, J. P., L. Tan, and S. Wang (2010), An isolated cohesive crack in tension, *Continuum Mech. Thermodyn.*, *22*, 617–634.

Dieterich, J. (1979), Modeling of rock friction: 1. Experimental results and constitutive equations, *J. Geophys. Res.*, *84*(15), 2161–2168.

Dieterich, J. H. (1992), Earthquake nucleation on faults with rate- and state-dependent friction, *Tectonophysics*, *211*, 115–134.

Di Toro, G., R. Han, T. Hirose, N. De Paola, S. Nielsen, K. Mizoguchi, F. Ferri, M. Cocco, and T. Shimamoto (2011), Fault lubrication during earthquakes, *Nature*, *471*, 494–498, doi:10.1038/nature09838.

Erdogan, F., G. D. Gupta, and T. S. Cook (1973), Numerical solution of singular integral equations, in *Mechanics of Fracture*, vol. 1, chap. 7, pp. 368–425, Noordhoff Int., Leyden, Netherlands.

Garagash, D. I. (2012), Seismic and aseismic slip pulses driven by thermal pressurization of pore fluid, *J. Geophys. Res.*, *117*, B04314, doi:10.1029/2011JB008889.

Garagash, D. I., and J. W. Rudnicki (2003), Shear heating of a fluid-saturated slip-weakening dilatant fault zone: 1. Limiting regimes, *J. Geophys. Res.*, *108*(B2), 2121, doi:10.1029/2001JB001653.

Garagash, D. I., L. N. Germanovich, L. C. Murdoch, S. Martel, Z. Reches, D. Ellsworth, T. C. Onstott, and S. D. Glaser (2009), A thermal technique of fault nucleation, growth, and slip, *Eos Trans. AGU*, *90*(52), Fall Meet. Suppl., Abstract H23E-0995.

Garagash, D. I., E. Detournay, and J. I. Adachi (2011), Multiscale tip asymptotics in hydraulic fracture with leak-off, *J. Fluid Mech.*, *669*, 260–297, doi:10.1017/S002211201000501X.

Germanovich, L. N., and R. A. Chanpura (2002), Modeling thin inclusions in poroelastic medium by line discontinuities, in *IUTAM Symposium on Analytical and Computational Fracture Mechanics of Non-Homogeneous Materials : proceedings of the IUTAM symposium held in Cardiff, U.K., 18-22 June 2001*, *Solid Mech. Appl.*, vol. 97, edited by B. L. Karihaloo, pp. 133–142, Kluwer Acad., Dordrecht, Netherlands.

Germanovich, L. N., L. C. Murdoch, D. I. Garagash, Z. Reches, S. J. Martel, D. Gwaba, D. Ellsworth, R. P. Lowell, and T. C. Onstott (2010), A controllable earthquake rupture experiment on the Homestake fault, Abstract H13F-1045 presented at 2010 Fall Meeting, AGU, San Francisco, Calif., 13–17 Dec.

Germanovich, L. N., L. C. Murdoch, D. I. Garagash, Z. Reches, S. J. Martel, D. Gwaba, D. Ellsworth, and T. C. Onstott (2011), Earthquake rupture experiment on the Homestake fault, paper presented at 2011 Engineering Research and Innovation Conference, Natl. Sci. Found., Atlanta.

Han, C., and I. Vardoulakis (1991), Plane-strain compression experiments on water-saturated fine-grained sand, *Geotechnique*, *41*, 49–78.

Hanks, T. C., and H. Kanamori (1979), Moment magnitude scale, *J. Geophys. Res.*, *84*(B5), 2348–2350, doi:10.1029/JB084iB05p02348.

Healy, J. H., W. W. Rubey, D. T. Griggs, and C. B. Raleigh (1968), The Denver earthquakes, *Science*, *161*, 1301–1310.

Herrmann, R. B., S.-K. Park, and C.-Y. Wang (1981), The Denver earthquakes of 1967–1968, *Bull. Seismol. Soc. Am.*, *71*(3), 731–745.

Hsieh, P. A., and J. D. Bredehoeft (1981), A reservoir analysis of the Denver earthquakes: A case of induced seismicity, *J. Geophys. Res.*, *86*(B2), 903–920.

Hubbert, M. K., and W. W. Rubey (1959), Role of fluid pressure in mechanics of overthrust faulting, 1. Mechanics of fluid-filled porous solids and its application to overthrust faulting, *Geol. Soc. Am. Bull.*, *70*, 115–166.

Ida, Y. (1972), Cohesive force across the tip of a longitudinal-shear crack and Griffith's specific surface energy, *J. Geophys. Res.*, *77*, 3796–3805.

Ionescu, I. R., and M. Campillo (1999), Influence of the shape of friction law and fault finiteness on the duration of initiation, *J. Geophys. Res.*, *104*, 3013–3024.

Kevorkian, J., and J. Cole (1996), *Multiple Scale and Singular Perturbation Methods*, Springer, New York.

King, F. W. (2009), *Hilbert Transforms*, vol. I, Cambridge Univ. Press, Cambridge, U. K.

Lachenbruch, A. H. (1980), Frictional heating, fluid pressure, and the resistance to fault motion, *J. Geophys. Res.*, *85*, 6097–6112.

Lachenbruch, A. H., and J. H. Sass (1980), Heat flow and energetics of the San Andreas fault zone, *J. Geophys. Res.*, *85*(B11), 6185–6223.

Lapusta, N., and J. R. Rice (2003), Low-heat and low-stress fault operation in earthquake models of statically strong but dynamically weak faults, *Eos Trans. AGU*, *84*(46), Fall Meet. Suppl., Abstract S51B-02.

Lapusta, N., J. R. Rice, Y. Ben-Zion, and G. Zheng (2000), Elastodynamic analysis for slow tectonic loading with spon- taneous rupture episodes on faults with rate- and state- dependent friction, *J. Geophys. Res.*, *105*(B10), 23,765–23,789, doi:10.1029/2000JB900250.

Marone, C. (1998), Laboratory-derived friction laws and their application to seismic faulting, *Annu. Rev. Earth Planet. Sci.*, *26*, 643–696.

Marone, C., B. E. Hobbs, and A. Ord (1992), Coulomb constitutive laws for friction: Contrasts in frictional behavior for distributed and localized shear, *Pure Appl. Geophys.*, *139*, 195–214.

McGuire, J. J., P. J. Shore, and M. G. Bevis (1997), The March 9, 1994 (Mw 7.6), deep Tonga earthquake: Rupture outside the seismically active slab, *J. Geophys. Res.*, *102*(B7), 15,163–15,182, doi:10.1029/96JB03185.

Muskhelishvili, N. (1977), *Singular Integral Equations*, Noordhoff Int., Leyden, Netherlands.

Noda, H., E. M. Dunham, and J. R. Rice (2009), Earthquake ruptures with thermal weakening and the operation of major faults at low overall stress levels, *J. Geophys. Res.*, *114*, B07302, doi:10.1029/2008JB006143.

Palmer, A. C., and J. R. Rice (1973), The growth of slip surfaces in the progressive failure of over-consolidated clay, *Proc. R. Soc. A*, *433*, 469–477.

Pearson, C. (1981), The relationship between microseismicity and high pore pressures during hydraulic stimulation experiments in low permeability granitic rocks, *J. Geophys. Res.*, *86*(B9), 7855–7864.

Platt, J., J. R. Rice, and J. W. Rudnicki (2010), Strain localization within a fluid-saturated fault gouge layer during seismic shear, *Eos Trans. AGU*, *90*(52), Fall Meet. Suppl., Abstract T31D-03.

Raleigh, C. B., J. H. Healy, and J. D. Bredehoeft (1976), An experiment in earthquake control at Rangely, Colorado, *Science*, *191*, 1230–1237.

Rempel, A. W., and J. R. Rice (2006), Thermal pressurization and onset of melting in fault zones, *J. Geophys. Res.*, *111*, B09314, doi:10.1029/2006JB004314.

Rempel, A. W., and S. L. Weaver (2008), A model for flash weakening by asperity melting during high-speed earthquake slip, *J. Geophys. Res.*, *113*, B11308, doi:10.1029/2008JB005649.

Rice, J. R. (1968), Mathematical analysis in the mechanics of fracture, in *Fracture, An Advanced Treatise*, vol. II, edited by H. Liebowitz, chap. 3, pp. 191–311, Academic, New York.

Rice, J. R. (1980), The mechanics of earthquake rupture, in *Physics of the Earth's Interior*, edited by A. Dziewonski and E. Boschi, pp. 555–649, North-Holland, Amsterdam.

Rice, J. R. (1992), Fault stress states, pore pressure distributions, and the weakeness of the San Andreas fault, in *Fault Mechanics and Transport Properties of Rock: A Festschrift in Honor of W. F. Brace*, edited by B. Evans and T.-F. Wong, pp. 475–503, Academic, San Diego, Calif.

Rice, J. R. (2006), Heating and weakening of faults durin earthquake slip, *J. Geophys. Res.*, *111*, B05311, doi:10.1029/2005JB004006.

Rice, J. R., and K. Uenishi (2010), Rupture nucleation on an interface with a power-law relation between stress and displacement discontinuity, *Int. J. Fracture*, *163*, 1–13, doi:10.1007/s10704-010-9478-5.

Rubin, A. M., and J.-P. Ampuero (2005), Earthquake nucleation on (aging) rate and state faults, *J. Geophys. Res.*, *110*, B11312, doi:10.1029/2005JB003686.

Rudnicki, J. W. (1999), Alteration of regional stress by reservoirs and other inhomogeneities: Stabilizing or destabilizing?, in *Proceedings of the Ninth International Congress on Rock Mechanics, Paris, France, August 25–28*, vol. 3, edited by G. Vouille and P. Berest, pp. 1629–1637, A.A. Balkema, Rotterdam, Netherlands.

Ruina, A. (1983), Slip instability and state variable friction laws, *J. Geophys. Res.*, *88*, 10,359–10,370.

Rummel, F., H. J. Alheid, and C. Frohn (1978), Dilatancy and fracture-induced velocity changes in rock and their relation to frictional sliding, *Pure Appl. Geophys.*, *116*, 743–764.

Rutledge, J. T., W. S. Phillips, and M. J. Mayerhofer (2004), Faulting induced by forced fluid injection and fluid flow forced by faulting: An interpretation of hydraulic-fracture microseismicity, Carthage Cotton Valley gas field, Texas, *Bull. Seismol. Soc. Am.*, *94*(5), 1817–1830.

Scholz, C. H. (1990), *The Mechanics of Earthquakes and Faulting*, Cambridge Univ. Press, Cambridge, U. K.

Segall, P. (1989), Earthquakes triggered by fluid extraction, *Geology*, *17*, 942–946.

Segall, P., and J. R. Rice (1995), Dilatancy, compaction, and slip instability of a fluid-infiltrated fault, *J. Geophys. Res.*, *100*, 22,155–22,171.

Segall, P., and J. R. Rice (2006), Does shear heating of pore fluid contribute to earthquake nucleation?, *J. Geophys. Res.*, *111*, B09316, doi:10.1029/2005JB004129.

Seno, T. (2005), Variation of downdip limit of the seismogenic zone near the Japanese islands: Implications for the serpentinization mechanism of the forearc mantle wedge, *Earth Planet. Sci. Lett.*, *231*, 249–262, doi:10.1016/j.epsl.2004.12.027.

Shapiro, S. A., R. Patzig, E. Rothert, and J. Rindschwentner (2003), Triggering of seismicity by pore-pressure perturbations: Permeability-related signatures of the phenomenon, *Pure Appl. Geophys.*, *160*, 1051–1066.

Shapiro, S. A., J. Kummerow, C. Dinske, G. Asch, E. Rothert, J. Erzinger, H.-J. Kumpel, and R. Kind (2006), Fluid induced seismicity guided by a continental fault: Injection experiment of 2004/2005 at the German deep drilling site (KTB), *Geophys. Res. Lett.*, *33*, L01309, doi:10.1029/2005GL024659.

Sibson, R. (1973), Interaction between temperature and fluid pressure during earthquake faulting—A mechanism for partial or total stress relief, *Nature*, *243*, 66–68.

Sibson, R. H. (1986), Rupture interaction with fault jogs, in *Earthquake Source Mechanics*, *Geophys. Monogr. Ser.*, vol. 37, edited by S. Das, J. Boatwright, and C. Scholz, pp. 157–168, AGU, Washington, D. C.

Sibson, R. H. (1992), Implications of fault-valve behaviour for rupture nucleation and recurrence, *Tectonophysics*, *211*, 283–293.

Townend, J., and M. D. Zoback (2004), Regional tectonic stress near the San Andreas fault in central and southern California, *Geophys. Res. Lett.*, *31*, L15S11, doi:10.1029/2003GL018918.

Tse, S., and J. R. Rice (1986), Crustal earthquake instability in relation to the depth variation of slip properties, *J. Geophys. Res.*, *91*, 9452–9472.

Uenishi, K., and J. R. Rice (2003), Universal nucleation length for slip-weakening rupture instability under nonuniform fault loading, *J. Geophys. Res.*, *108*(B1), 2042, doi:10.1029/2001JB001681.

Viesca, R. C. (2011), The near and far of pore pressure during landslide and earthquake ruptures, PhD thesis, Harvard Univ., Cambridge Mass.

Viesca, R. C., and J. R. Rice (2012), Nucleation of slip-weakening rupture instability in landslides by localized increase of pore pressure, *J. Geophys. Res.*, *117*, B03104, doi:10.1029/2011JB008866.

Walder, J., and A. Nur (1984), Porosity reduction and pore pressure development, *J. Geophys. Res.*, *89*, 11,539–11,548.

Warpinski, N. R., and L. W. Teufel (1987), Influence of geologic discontinuities on hydraulic fracture propagation, *J. Pet. Technol.*, *39*, 209–220.

Wibberley, C. A. J. (2002), Hydraulic diffusivity of fault gouge zones and implications for thermal pressurization during seismic slip, *Earth Planets Space*, *54*, 1153–1171.

Wibberley, C. A. J., and T. Shimamoto (2003), Internal structure and permeability of major strike-slip fault zones: The median tectonic line in Mie prefecture, southwest Japan, *J. Struct. Geol.*, *25*(1), 59–78.

Wong, T. F. (1986), On the normal stress dependence of the shear fracture energy, in *Earthquake Source Mechanics*, *Geophys. Monogr. Ser.*, vol. 37, edited by S. Das, J. Boatwright, and C. H. Scholz, pp. 1–11, AGU, Washington, D. C.

Wong, T.-F., S.-C. Ko, and D. L. Olgaard (1997), Generation and maintenance of pore pressure excess in a dehydrating system: 2. Theoretical analysis, *J. Geophys. Res.*, *102*(B1), 841–852.

Zoback, M. D., and H.-P. Harjes (1997), Injection-induced earthquakes and crustal stress at 9 km depth at the KTB deep drilling site, Germany, *J. Geophys. Res.*, *102*(B8), 18,477–18,491.